Investigating the Dynamics of the Interaction between Mammalian Host Organelles and *Toxoplasma*

By

Luqiong Wang

A thesis submitted to Johns Hopkins University in conformity with the requirements for the Degree of Master of Science

Baltimore, Maryland

April, 2019

ABSTRACT

Toxoplasma gondii is an intracellular protozoan parasite that infects roughly one-third of the world population. Although infection in healthy individuals is generally asymptomatic, it may cause severe health issues in immunocompromised patients. During invasion of a mammalian cell, *T. gondii* establishes a parasitophorous vacuole (PV) which is separated from the host cytoplasm by the PV membrane (PVM). The PVM forms a critical barrier between *T. gondii* and the infected cell and is involved in the manipulation of host cellular functions, including signaling and nutrient acquisition. Previous fluorescence and electron microscopic observations have shown that the parasites are able to intercept host Rab trafficking pathways and internalize host Rab vesicles (e.g., Rab11 vesicles for the recycling pathway) into the PV, but these findings are based on fixed cells. What is missing is a dynamic view of the PVM and its interaction with host Rab vesicles by live cell imaging. This dynamic view of the PVM will help us to understand the mechanism of host vesicle internalization by PVM. Therefore, the aim of this thesis is to analyze the dynamics of the PVM over time relative to host Rab vesicles.

To do so, we selected two PVM proteins, GRA3 and GRA7. We endogenously tagged GRA3 and GRA7 with the fluorescent marker mCherry using CRISPR/Cas9 gene editing. Both GRA3 and GRA7 are highly expressed and secreted from the parasite's dense granule secretory organelles into the PV where they localize to the PVM and an intravacuolar network of membranous tubules (IVN), which has been proposed to be involve in host Rab vesicle internalization into the PV. The functional characteristics of GRA3-mCherry and GRA7-mCherry expressing strains were evaluated by intracellular growth assays, localization assay and live cell imaging. The insertion of mCherry at the 3' end of GRA3

does not interfere with the intracellular replication of the parasite, or the localization of GRA3 to the dense granules, PVM and IVN. Though insertion of mCherry at the 3'end of GRA7 does not interfere with the growth of the parasite, but it affects the localization of GRA7 to the dense granules, PVM and IVN, and it is most likely cleaved from GRA7 inside the parasite.

Using the GRA3-mCherry expressing strains, we observed that PVM projections (PVMP) are a dynamic feature of the PV, with projections extending into the host cytosol and then retracting. To study interactions between host vesicles and the PVM, we infected cells stably expressing GFP-Rab11A with GRA3-mCherry expressing parasites and we observed that host Rab11A vesicles inside the PV either remained unmoving in the IVN region or were transported along the IVN, indicating a role of the IVN in sequestering and transporting host vesicles inside the PV. We also observed that host Rab11A vesicles contact the PVM, with some vesicles entering the PV, though the moment of entry was not captured due to technical complications due to long exposure times leading to fading of the GFP signal. The GRA3-mCherry expressing strains generated from our study will also be a valuable tool to study various interactions between the PVM and many different host organelles, including how PVMPs interact with host organelles.

1st reader/advisor: Dr. Isabelle Coppens

2nd reader: Dr. Anne Hamacher-Brady

ACKNOWLEDGMENT

First, I would like to express my very profound gratitude to Dr. Isabelle Coppens for giving me this great opportunity to work in her lab and participate in this exciting project. I thank Isabelle for her generous support to my master's training at Johns Hopkins University School of Public Health. Without her support, I would not have been able to overcome difficulties in my life and have such accomplishments for my master's training. I also thank Isabelle for being an excellent research advisor, for her help with this thesis, as well as my transition to the next position.

I would like to thank the members of the Coppens Lab: Julia Romano, Karen Ehrenman, Eric Hartman, Tejram Sahu and Ella Gehrke. I specially thank Julia, who I closely worked with, for her endless help not only in research but also in life. She is an excellent research mentor and life advisor. I also thank Julia for her help in editing and providing insightful comments for this thesis. I thank Karen for her patience to answer many of my questions and for her help with my experiments. I thank Eric, Tejram and Ella, for their help, support and advise during my time in the lab. I feel very lucky to join such a supportive and friendly lab.

I want to thank Anne Hamacher-Brady in the Department of Molecular Microbiology and Immunology for her time and effort being the secondary reader on my thesis. Her insightful comments were a huge benefit to my thesis. I would also like to thank Tim Wang from the Brady's lab for his help with live cell imaging and ImageJ.

I would like to acknowledge our collaborators. Dr. Vern Carruthers from the University of Michigan for providing the *ΔKu80Δhxgprt* parasite strain; Dr. David Sibley

from the Washington University in St. Louis for the pSAG1::CAS9-U6::UPRT plasmid; and Dr. David Roos from the University of Pennsylvania for the pminiHXGPRT plasmid.

I would like to thank Gail O'Connor, the academic program administrator, for her help with all works related to academic and degree requirements. I also want to thank all of the people I met at Hopkins for their advice, help and support.

Finally, I would like to thank my parents and friends for providing me with endless support, both spiritually and financially, throughout my years of studying abroad. This accomplishment would not have been possible without them.

TABLE OF CONTENTS

LIST OF TABLES

LIST OF FIGURES

LIST OF ABBREVIATIONS USED

1. PV-parasitophorous vacuole
2. PVM-parasitophorous vacuole membrane
3. PVMP- parasitophorous vacuole membrane projection
4. AMA1– apical membrane antigen 1
5. RON2– rhoptry-derived proteins 2
6. IVN-intravacuolar network
7. ER-endoplasmic reticulum
8. MTOC-microtubule-organizing center
9. GRA-dense granule protein
10. CRISPR-clustered regularly interspaced short palindromic repeats
11. sgRNA-single guide RNA
12. PAM-protospacer adjacent motif
13. DSB-double strand break
14. NHEJ-non-homologous end joining
15. HFF-human foreskin fibroblast
16. IFA-immunofluorescence assays
17. PCCs-Pearson's correlation coefficients
18. PDM-product of the difference of the means
19. HXGPRT-hypoxanthine-xanthine-guanine phosphoribosyl transferase
20. PCR-polymerase chain reaction

1. INTRODUCTION:

Toxoplasma gondii is an obligate intracellular parasite that infects nearly all warm-blooded animals and invades any nucleated cells, which makes it as one of the most successful and widespread parasites on earth. It has been estimated that *Toxoplasma* infects roughly one-third of the world population, with a prevalence that varies widely from 10% to 80% between countries (Robert-Gangneux and Dardé, 2012). Acute infection (corresponding to the proliferative phase of the parasite in the small intestine) resulting from ingestion of the parasite cysts from contaminated food or water, or infected cat feces usually causes no or mild flu-like symptoms, but the parasite forms cysts in various body tissues that results in life-long chronic infection. However, although chronic infection with *T. gondii* is generally asymptomatic in healthy individuals, reactivation of the cysts can cause devastating ocular, neurological and systemic diseases, most often in immunocompromised individuals such as HIV/AIDs patients and in organ transplant recipients (Munoz et al., 2010; Wang et al., 2017). In addition, *T. gondii* can be congenitally passed from pregnant women through the placenta to the fetus, resulting in blindness, cognitive impairment, hydrocephalus or abortion (Mastroiacovo & Torgerson, 2013).

Current therapy for *Toxoplasma* infection only controls acute infections and is associated with adverse reactions. For example, it is recommended to treat toxoplasmosis using a combination of pyrimethamine and sulfadiazine which inhibit parasite folate metabolism (Rajapakse et al., 2013). However, pyrimethamine and sulfadiazine have significant adverse effects by decreasing red blood cells, white blood cells and platelets (Neville et al., 2015; Montazeri et al., 2017). There currently is no drug to clear the chronic cyst form and no vaccine to prevent *T. gondii* infections. Due to the high prevalence and

life-long threat of *T. gondii* infection, new strategies and therapeutic drugs are needed to prevent and treat both *T. gondii* acute and chronic infections.

A. Life cycle and transmission of *T. gondii*

T. gondii has a complex life cycle with a sexual cycle in the definitive host (felids), and an asexual cycle in intermediate hosts (warm-blooded animals) (Figure 1). In the sexual cycle, a cat (domestic and wild) ingests tissue cysts from the skeletal muscle, heart and brains of an infected intermediate host. The tissue cyst wall is dissolved by proteolytic enzymes in the cat's stomach and small intestine, releasing bradyzoites from the cyst that infect the epithelial cells of the cat's small intestine. The bradyzoites invade epithelial cells and differentiate into merozoites, reproduce rapidly and give rise to male and female gametes, which fuse together to form a zygote and mature as an oocyst (Ferguson, 2004). The oocyst is passed through cat feces and sporulates in the environment to become highly infectious. It can be widely spread to contaminate water, soil, or food, and can survive in old and dry environment for years (Dubey et al., 2011). In intermediate hosts (all warm-blooded animals), *T. gondii* oocysts or tissue cysts release sporozoites and bradyzoites, respectively, which infect intestinal epithelial cells. The parasites convert to the fast-growing tachyzoite form that disseminates throughout the body. Due to pressure from the host immune responses to infection, tachyzoites convert to bradyzoites and form tissue cysts (Miller et al., 2009). These cysts can be found in various tissues inside host body, predominantly in skeletal muscle, heart, brain and eye tissues (Kim & Weiss, 2011).

Consumption of undercooked meat with tissue cysts is one of the major ways of *T. gondii* infection, both in human and meat-eating animals, as well as ingestion of oocyst-

contaminated water, soil, or food. In fact, *Toxoplasma* is a major cause of food-borne illness (Hussain et al., 2017). Humans can also pick up oocysts from the litter boxes of infected indoor or outdoor cats. Therefore, pregnant women are advised not to clean cat litter boxes during the pregnancy as a prevention of *T. gondii* infection. In the United States, oocysts are the major source of congenitally transmitted *T. gondii* infection, which leads to severe health consequences for the fetus (Boyer et al., 2011).

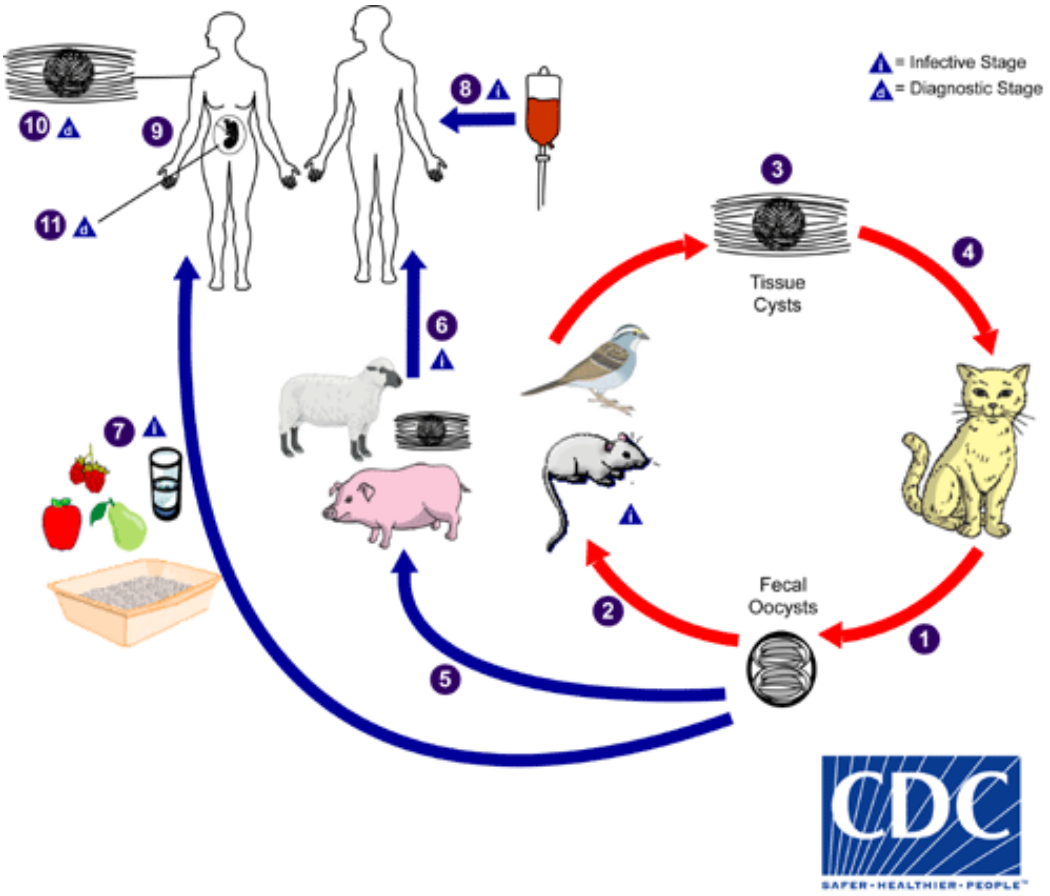

Figure 1-Transmission of *T. gondii* in intermediate and definitive hosts. Felidae such as cats are the only known definitive hosts for *T. gondii*, who shed highly infectious oocysts in the environment. Humans can be infected by *T. gondii* by ingesting oocysts from infected cat, contaminated food and water, and eating poorly cooked meat with tissue cysts. In some rare cases, *T. gondii* is transmitted through organ transplantation. In pregnant women, *T. gondii* can be congenitally transmitted to the fetus. (CDC, taken from: https://www.cdc.gov/parasites/toxoplasmosis/biology.html)

B. Intracellular invasion of *T. gondii*

Host cell invasion is essential for *T. gondii* as a survival strategy because it is an obligate intracellular parasite (Kafsack et al., 2009). There are multiple steps for host cell invasion by *T. gondii* (Figure 2).

When *T. gondii* infects a host cell, it first attaches, using its apical end, to the host cell plasma membrane. The apical end contains secretory organelles, such as micronemes and rhoptries, that secretes parasite proteins, such as apical membrane antigen 1 (AMA1) and rhoptry-derived proteins 2 (RON2), to create a ring like moving junction (Tonkin et al., 2011). The moving junction mediates the invagination of the host cell plasma membrane, which surrounds the parasites to form a parasitophorous vacuole (PV), and it excludes transmembrane host proteins from the PV membrane (PVM) but contains many proteins secreted by the parasite, creating a unique niche for the parasite inside the host cytosol (Sibley et al., 1999; Sibley and Charron, 2004). The PVM does not fuse with any host organelles (non-fusogenic) and forms a critical barrier between *T. gondii* and the host cytoplasm, protecting parasites from host attack mechanisms. For example, studies have shown that the PVM, lacking host endocytic markers, helps protect the PV from fusion and destruction by host lysosomes (Mordue et al., 1999). The PVM is also involved in manipulation of host cellular functions, such as NF-kB signaling and nutrient acquisition (Molestina et al., 2003; Sinai et al.,2007), but the molecular players of these manipulations remain largely unknown.

After invasion of the host cell, the PVM interacts and associates with several host organelles, including the endoplasmic reticulum (ER), microtubules, Golgi and mitochondria (de Melo et al., 1992; Walker et al., 2008; Romano et al., 2013). The parasite

replicates asexually by endodyogeny around every eight hours. In the process of endodyogeny, two daughter cells are formed within the mother cell, which is consumed by the daughters before their separation. This process continues until the host cell is filled with parasites (Blader et al., 2015).

Parasites then egress from the host cell after the breakdown of the host cell plasma membrane in response to K+ and Ca+ ion fluxes (Kafsack et al., 2009). Indeed, previous studies have shown that the mechanical pressure of the PV leads to an ionic imbalance, which triggers the egress of *T. gondii* (Moundy et al., 2001). In response to the ion imbalance, the parasites secrete perforins that permeabilize the PVM (Kafsack et al., 2009). The *Toxoplasma* Ca^{2+}-dependent protein kinase 3 (TgCDP3), which responds to cytoplasmic Ca^{2+} ions, is also important to regulate egress through the phosphorylation of the parasite's actin-myosin motor leading to the activation of parasite motility for movement out of the host cell (Tonkin et al., 2012; Gaji et al., 2015).

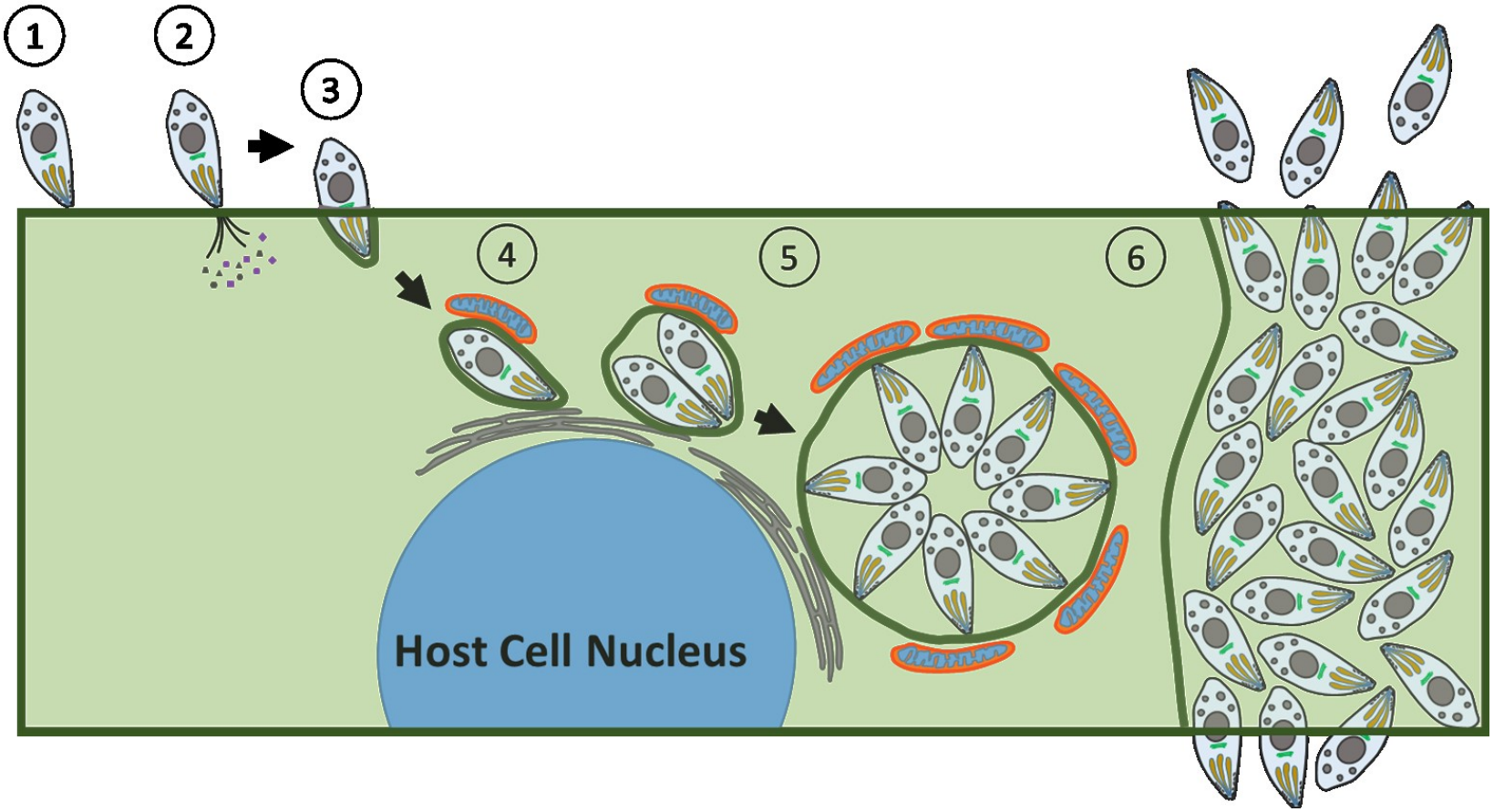

Figure 2-Intracelullar parasitism of *T. gondii.* ①attachment to the host cell plasma membrane. ② secretion of *Toxoplasma* proteins to make a moving junction. ③Invagination of host plasma membrane and creation of PVM (dark green) during invasion. ④ Formation of PV, which associates with host organelles such as mitochondria and ER. ⑤ Replication of *T. gondii* inside the PV by endodyogeny. ⑥ Egress of *T. gondii* from the PV and the host cell.

C. Scavenging of host nutrients

As an obligate intracellular parasite, *T. gondii* needs to rely on its host for nutrients to survive and replicate. Essential nutrients for *T. gondii* include tryptophan (Pfefferkorn, 1984), arginine (Fox et al., 2004), polyamines (Seabra et al., 2004), purines (Schwartzman and Pfefferkorn, 1982), cholesterol (Coppens and Joiner, 2003), iron (Dimier and Bout, 1998) and other lipids (Sibley and Charron, 2002). Though the PVM provides a protective barrier for *T. gondii*, its non-fusogenic property also poses a challenge for the parasite to get access of nutrients from the host. At least, the PVM has small pores that allows small solutes less than 3kDa, such as NTPs, glucose, amino acids, to passively diffuse into the PV (Schwab et al., 1994; Gold et al., 2015). To obtain nutrients for host organelles, *T. gondii* has adopted a unique strategy: association of host organelles with the PVM followed by their sequestration into the PV lumen (Coppens, 2014).

Host mitochondria are a site of lipid metabolism, which may provide molecules such as ATP and lipids for *T. gondii* (Coppens, 2014). In fact, *T. gondii* scavenges lipoate from host mitochondria (Crawford et al, 2006). The host Golgi provide sphingolipids and studies have shown that the growth of *T. gondii* is decreased in cells impaired for sphingolipid production (Pratt et al., 2013; Romano et al., 2013). The host microtubular network plays an important role in the movement of membrane-bound compartments such as endosomes and lysosomes (Coppens et al., 2006). To recruit host endocytic compartments and Golgi vesicles, *T. gondii* reorganizes the microtubular network around the PV by associating with the microtubule-organizing center (MTOC) and the Golgi. Sphingolipids produced in the host Golgi and LDL cholesterol in host endolysosomes are transported to the PV (de Melo and De Souza, 1996; Coppens et al., 2000; Romano et al., 2013). Previous evidence from

the Coppens lab has shown that the parasite is able to intercept host Rab trafficking pathways and internalize host Golgi Rab vesicles into the PV (Figure 3) to acquire sphingolipids (Romano et al., 2017; Romano et al., 2013), but the molecular mechanisms of host vesicle internalization into the PV remains unknown. The PVM is hypothesized to play a role in these functions; indeed, this membrane forms long tubule extensions upon to 50 μm that pervade the host cytosol and contact host organelles (Dubremetz et al., 1993; Jacobs et al., 1998; Rome et al., 2008; Coppens et al., 2006; Romano et al., 2013; Romano et al., 2017). Within the PV lumen, membranous tubules initially secreted by the parasite form an entangled network, named the intravacuolar network (IVN) as shown in Figure 4 (Sibley et al., 1995). Some of these IVN tubules attach to the PVM and contain host organelles in their lumen, suggesting that the PVM and IVN contribute to the internalization of host organelles within the PV by forming conduits; in fact, parasite mutants defective in the IVN internalize fewer host organelles (Romano et al., 2017). These findings are based on fixed cells analyzed by immunofluorescence and electron microscopy. What is missing is a dynamic view of the PVM and its interaction with host Rab vesicles by live cell imaging. The activities at the PVM are likely plastic, reflecting temporal changes of host organelle attraction to the PV and then penetration into the vacuole.

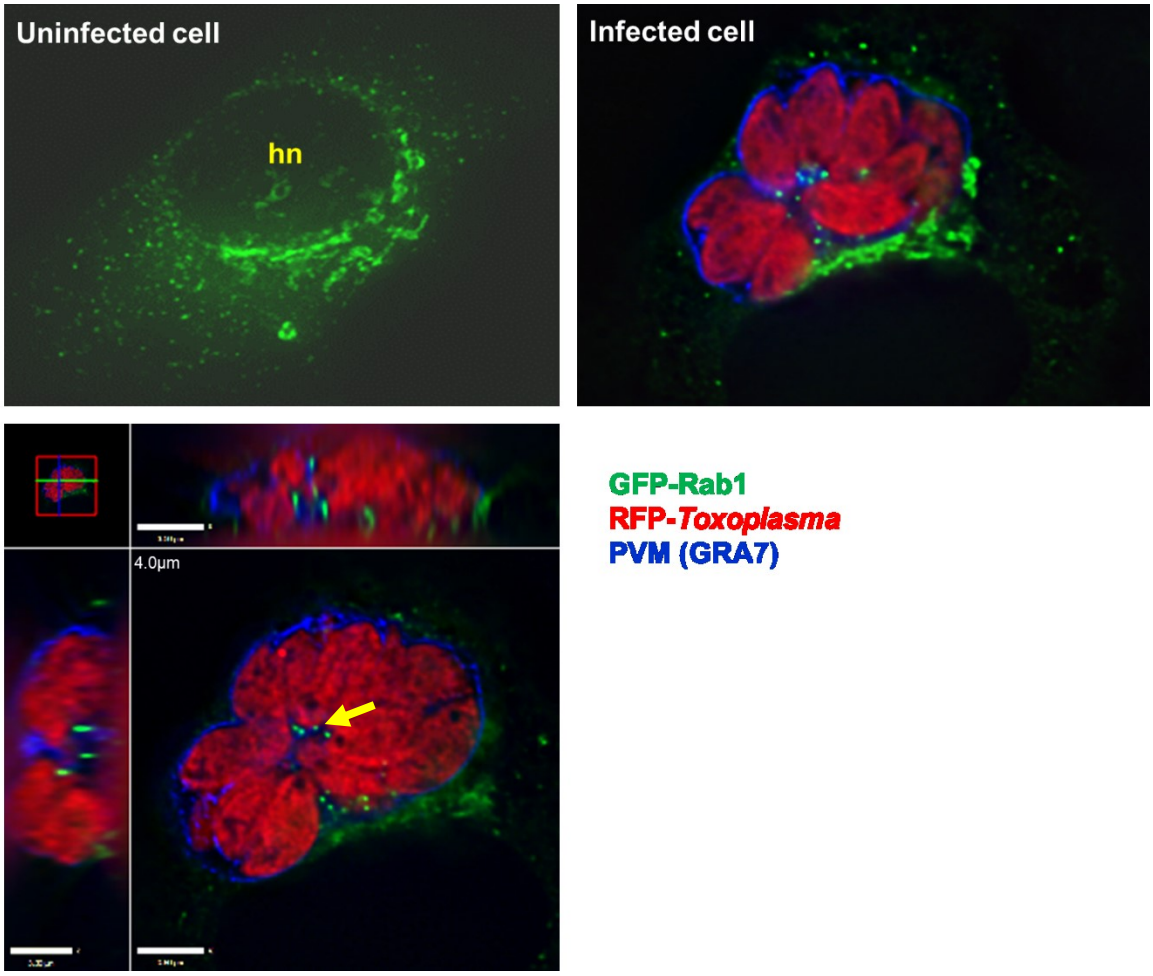

Figure 3-Attraction and sequestration of host Rab1 vesicles into the PV of *Toxoplasma*. Rab1 vesicles shuttle between the ER and the cis-Golgi and localize to these compartments in uninfected cells as seen in mammalian cells expressing GFP-Rab1. Upon infection, GFP-Rab1 vesicles concentrate around the PV (orange arrow) and are trapped inside the PV (yellow arrow), as confirmed by the orthogonal views. Taken from Romano et al., 2017

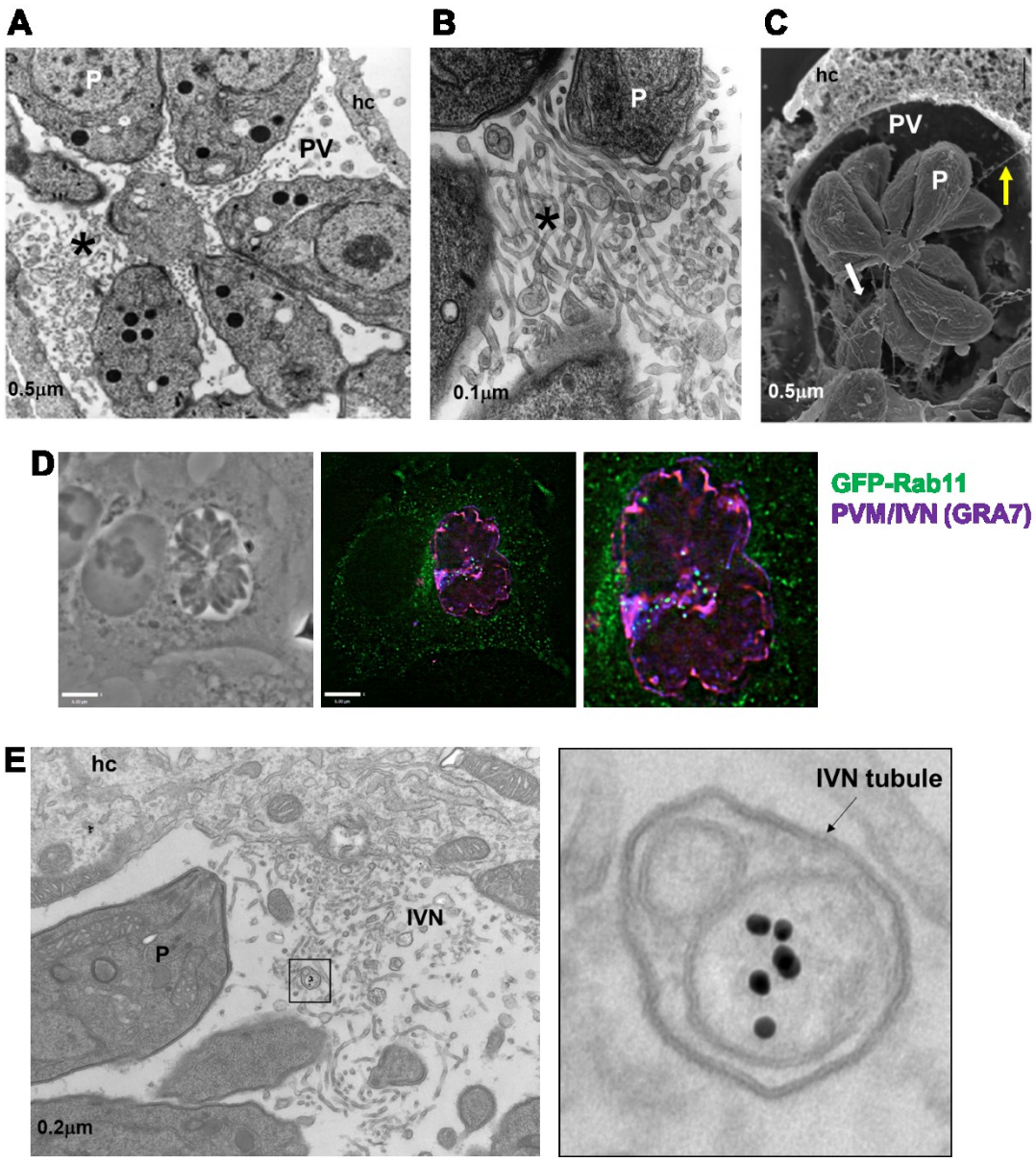

Figure 4-Role of the IVN in host organelle sequestration into the PV of *Toxoplasma.* **A-B.** Transmission EM showing the IVN labeled with an asterisk (Romano et al., 2017). P, parasite; hc, host cell. **C**. Scanning EM of the PV showing the IVN (white arrow) and a tubule of the IVN (yellow arrow) attached to the PVM (Magno et al., 2005). **D.** IFA of infected cells expressing GFP-Rab11, showing Rab11 vesicles concentrated to the IVN. (Romano et al., 2017) **E.** Transmission EM of mammalian cells incubated with LDL-gold particles to label endocytic organelles. LDL-containing organelles are seen inside a tubule (arrow) of the IVN. (Romano et al., 2017)

D. Dense granule proteins

T. gondii contains secretory organelles called dense granules that secrete proteins (GRA) into the PV. (Carruthers and Sibley, 1997). These proteins are important for maintaining the PV environment for *T. gondii* intracellular survival and replication (Nam, 2009). Some GRA proteins are able to traffic beyond the PV into the host cytoplasm or nucleus, and interfere with host cell signaling pathways and gene expression. For example, GRA15 activates the NF-kB pathway, which induces IL-12 production (Rosowski et al., 2011). GRA6 manipulates host immune responses by activating NFAT4, the host transcription nuclear factors of activated T cells 4 (Ma et al., 2014).

Inside the PV, some soluble GRAs localize to the PV lumen, and membrane-associated GRAs traffic to the PVM or IVN (Rome et al., 2008). For example, GRA1 is secreted within the vacuolar space of the PV. Vaccine studies indicate that GRA1 is a promising immunogenic candidate because it can induce an immunodominant response (Beghetto et al., 2001). Gene knockout studies have shown that GRA2 and GRA6 localize to the IVN, and are essential for IVN biogenesis (Mercier et al., 2002). Many membrane-associated GRA proteins are type 1 transmembrane proteins that traffic to the PVM (shown in Figure 5), and can contact both the vacuolar space of the PV and the host cytoplasm (Rome et al., 2008).

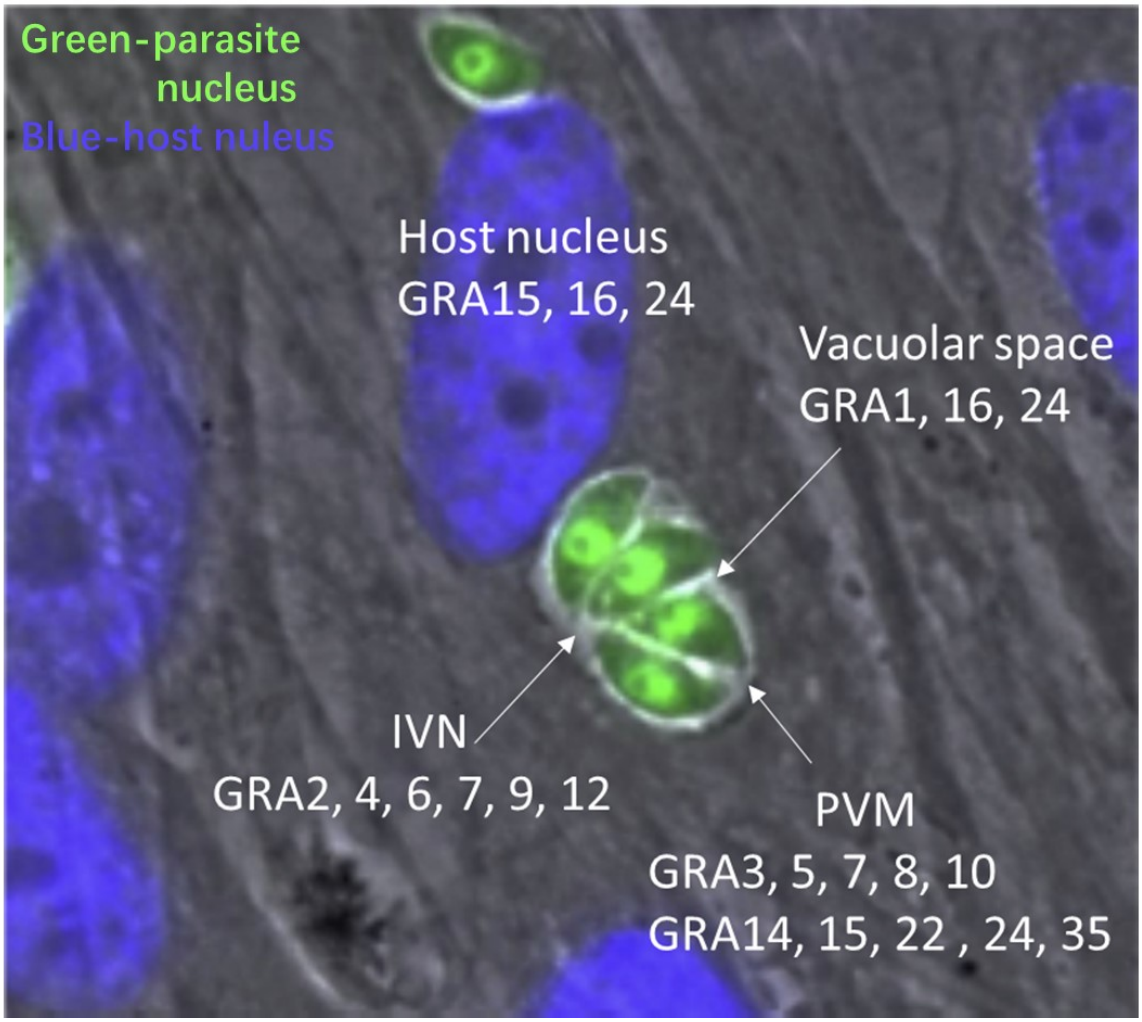

Figure 5-Localization of GRAs in *T. gondii* PV and host cells. GRAs are secreted from dense granules inside the parasite, and localize to the IVN (GRA 2,4,6,7,9,12), vacuolar space (GRA1,16,24), PVM (GRA3,5,6,8,10,14,15,22,24,40) and host nucleus (GRA15,16,24). Parasite nucleus (green), host nucleus (blue). Taken from Mercier and Cesbron-Delauw, 2015.

.

E. Gene editing of *T. gondii*

Clustered regularly interspaced short palindromic repeats (CRISPR) together with the Cas 9 enzyme form a naturally occurring system that is used as a defense mechanism in bacteria and archaea (Barrangou et al., 2007). Since its discovery, the CRISPR/Cas9 system has been widely adapted for editing genes in many organisms. This system is very efficient for targeted gene disruption and site-specific insertion through homologous recombination (Shen et al., 2014). In the CRISPR/Cas9 system, Cas9 nuclease is guided by a single guide RNA (sgRNA) targeting a specific site in the genome. It binds to the Protospacer adjacent motif (PAM) sequence, which follows the targeting site, and generates a double strand break (DSB) in the targeting site. Subsequently, cellular pathways are activated to repair the DSB, including non-homologous end joining (NHEJ), homologous repair (HR), or other alternative repair pathways (Figure 6; Cribbs and Perera, 2017). The CRISPR/Cas system has been used to efficiently mediate gene editing of *T. gondii*, including gene disruption (Bai et al., 2018; Wang et al., 2016) and complementation (Shen et al., 2017).

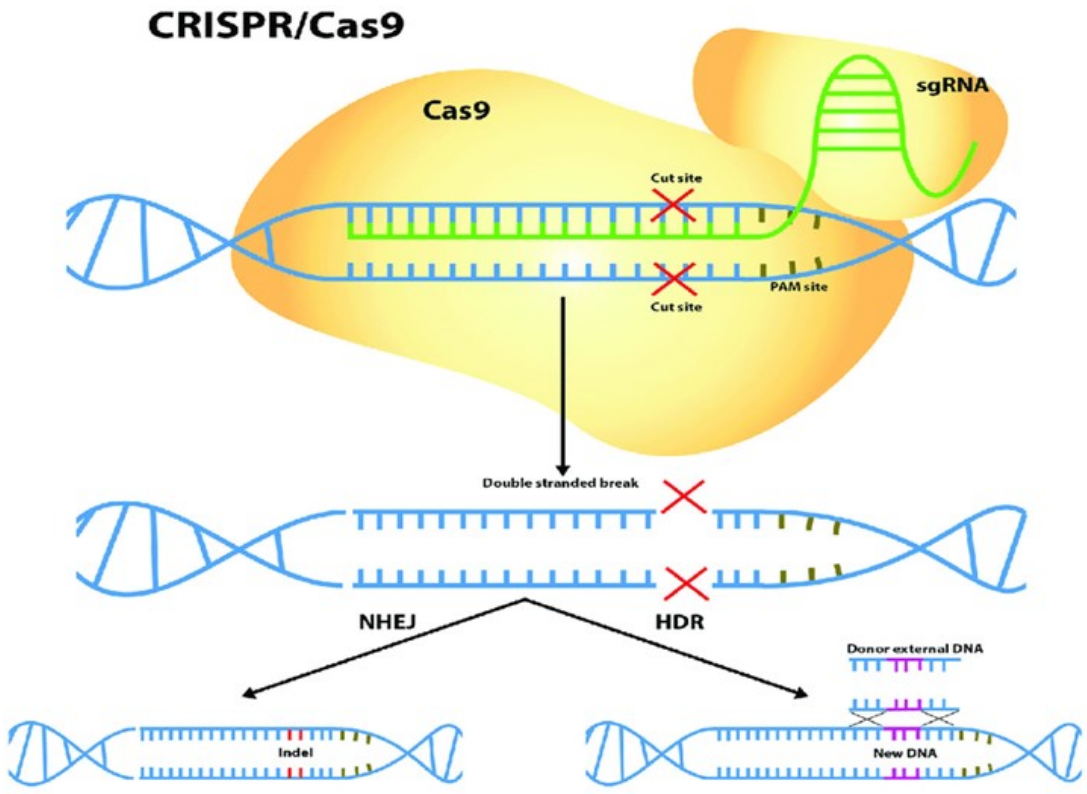

Figure 6-Mechanisms of CRISPR-Cas9 mediated gene editing. sgRNA recognizes a specific site in the genome, which recruits the Cas9 endonuclease. Binding of Cas9 endonuclease introduce a DBS, which is repaired by subsequent cellular repair including non-homologous end joining (NHEJ) or homology directed repair (HDR). Taken from Cribbs and Perera, 2017.

F. Study goal

Previously it was shown that *T. gondii* intercepts host Rab trafficking pathways and internalizes host Rab vesicles into the PV (Figure 3). As the PVM is non-fusogenic, but host vesicles are observed inside the PV, the mechanism of entry of host vesicles into the PV is enigmatic. EM observations suggest that IVN tubules are involved in vesicle internalization by attaching to the PVM and forming conduits. To further explore this possible scenario, we need a dynamic view to of the interactions between host vesicles and the PVM.

In the present study, we thus explored the interactions between host vesicles and PVM through live cell imaging. To achieve this goal, we adopted the CRISPR/Cas9 system to engineer *Toxoplasma* strains that stably express a mCherry-labeled dense granule protein, GRA3 or GRA7. These two proteins are highly expressed and localize to the PVM and IVN. I used these strains for live cell imaging to observe the interaction between host GFP-Rab11 vesicles and the PVM. Those parasite strains will also be valuable as a tool to study various interactions between PVM and any host organelles in future research.

2. MATERIAL AND METHODS:

A. Reagents and antibodies

All reagents were purchased from Sigma (St. Louis, MO) or Thermo Fisher Scientific (Waltham, MA), unless otherwise stated. The primary antibodies used for immunofluorescence assays (IFA) were monoclonal mouse anti-GRA3 provided by J.F. Dubremetz (Université of Montpellier, Montpellier, France) and polyclonal rabbit anti-GRA7 (Coppens et al., 2006). Secondary antibodies used were anti-mouse and anti-rabbit conjugated to Alexa Fluor 488 (Invitrogen, Carlsbad, CA). The primary antibodies used for western blot analysis were monoclonal mouse anti-GRA3, rabbit polyclonal anti-GRA7 and polyclonal rabbit anti-DsRed (Takara Bio, Mountain View, CA). The secondary antibodies used were horseradish peroxidase-conjugated goat anti-mouse and donkey anti-rabbit IgG (GE Health Care, UK).

B. Mammalian cell and parasite cultures

Human foreskin fibroblasts (HFF) were purchased from the American Type Culture Collection (Manassas, VA) and grown as monolayers. VERO cells stably expressing GFP-Rab11A were generated previously (Romano et al., 2017). All cells were maintained at 37°C in 5% CO_2 and cultivated in alpha-minimum essential medium (Alpha MEM) supplemented with 10% fetal bovine serum (FBS), 2mM glutamine, and penicillin/streptomycin (100 units/ml per 100 µg/ml). The tachyzoite form of *Toxoplasma* strain RH was used throughout this study including: *ΔKu80Δhxgprt* (Huynh and Carruthers, 2009), *GRA3-mCherry* and *GRA7-mCherry*.The parasites were propagated in vitro through serial passage in HFF monolayers (Khan and Grigg, 2017).

C. Construction of Plasmids

All plasmids, primers and sgRNAs used in this study are listed in Table I. We used CRISPR/Cas9 gene editing to tag *GRA3* or *GRA7* in the genome with mCherry. Guide RNA (gRNA) of *GRA3* or *GRA7* was designed using two websites, Eukaryotic Pathogen CRISPR guide RNA/DNA Design Tool (http://grna.ctegd.uga.edu/) and E-CRISPR (http://www.e-crisp.org/E-CRISP/). The GRA3 or GRA7 gRNA was engineered into plasmid pSAG1::CAS9-U6::sgUPRT (Shen et al., 2017) to replace UPRT sgRNA by using the Q5 Mutagenesis Kit (NEB, Ipswich, MA), and to generate pSAG1::CAS9-U6::sgGRA3 or pSAG1::CAS9-U6::sgGRA7 (Figure 7). Positive plasmids were extracted with the QIAprep Spin Miniprep Kit (Hilden, Germany) and confirmed by DNA sequencing.

To generate the GRA3-mCherry targeting plasmid, the pminiHXGPRT plasmid (Donald et al., 1996) was used as the backbone. *GRA3* from plasmid pTUB-GRA3-YFP (unpublished plasmid created previously in the laboratory), *mCherry* from plasmid pmCherry-Cl (Takara Bio, Japan), *DHFR 3'UTR* from pminiHXGPRT and *GRA3'3UTR* from genomic DNA of RH strain were amplified by PCR using the Expand High Fidelity PCR kit (Roche, Switzerland); primers used for PCR were shown in Table II. The PCR products were assembled into the pminiHXGPRT using the HIFI assembly Kit (NEB, Ipswich, MA) to generate the targeting plasmid, GRA3-mCherry-HXGPRT-GRA3 3'UTR (Figure 8). Positive plasmids were screened for by colony PCR, extracted with QIAprep Spin Miniprep Ki and confirmed by sequencing. The same method was used to create the GRA7-mCherry targeting plasmid, GRA7-mCherry-HXGPRT-GRA7 3'UTR. Both targeting plasmids were digested with the restriction enzymes *Kpn*l and *Xba*l (NEB,

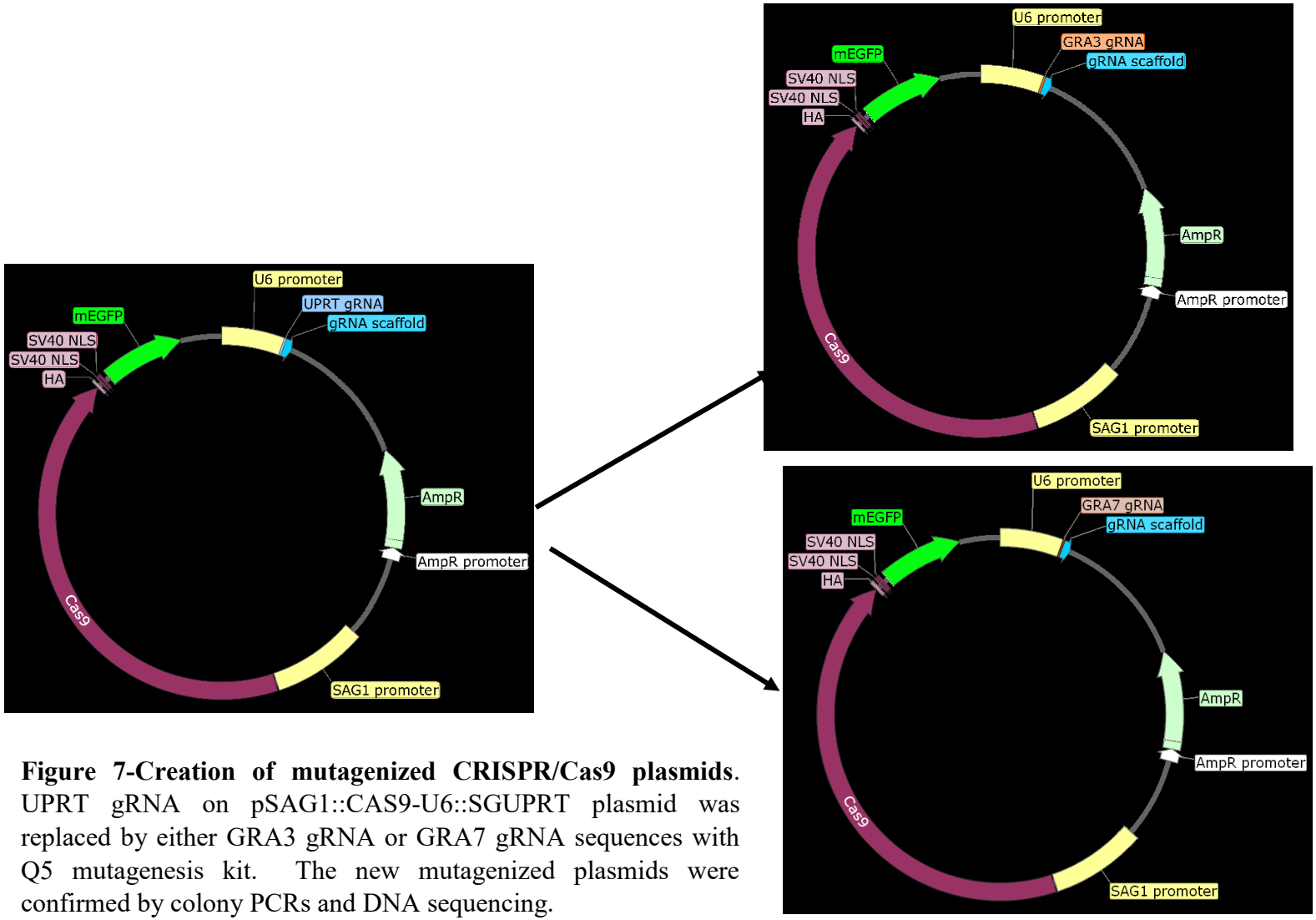

Figure 7-Creation of mutagenized CRISPR/Cas9 plasmids. UPRT gRNA on pSAG1::CAS9-U6::SGUPRT plasmid was replaced by either GRA3 gRNA or GRA7 gRNA sequences with Q5 mutagenesis kit. The new mutagenized plasmids were confirmed by colony PCRs and DNA sequencing.

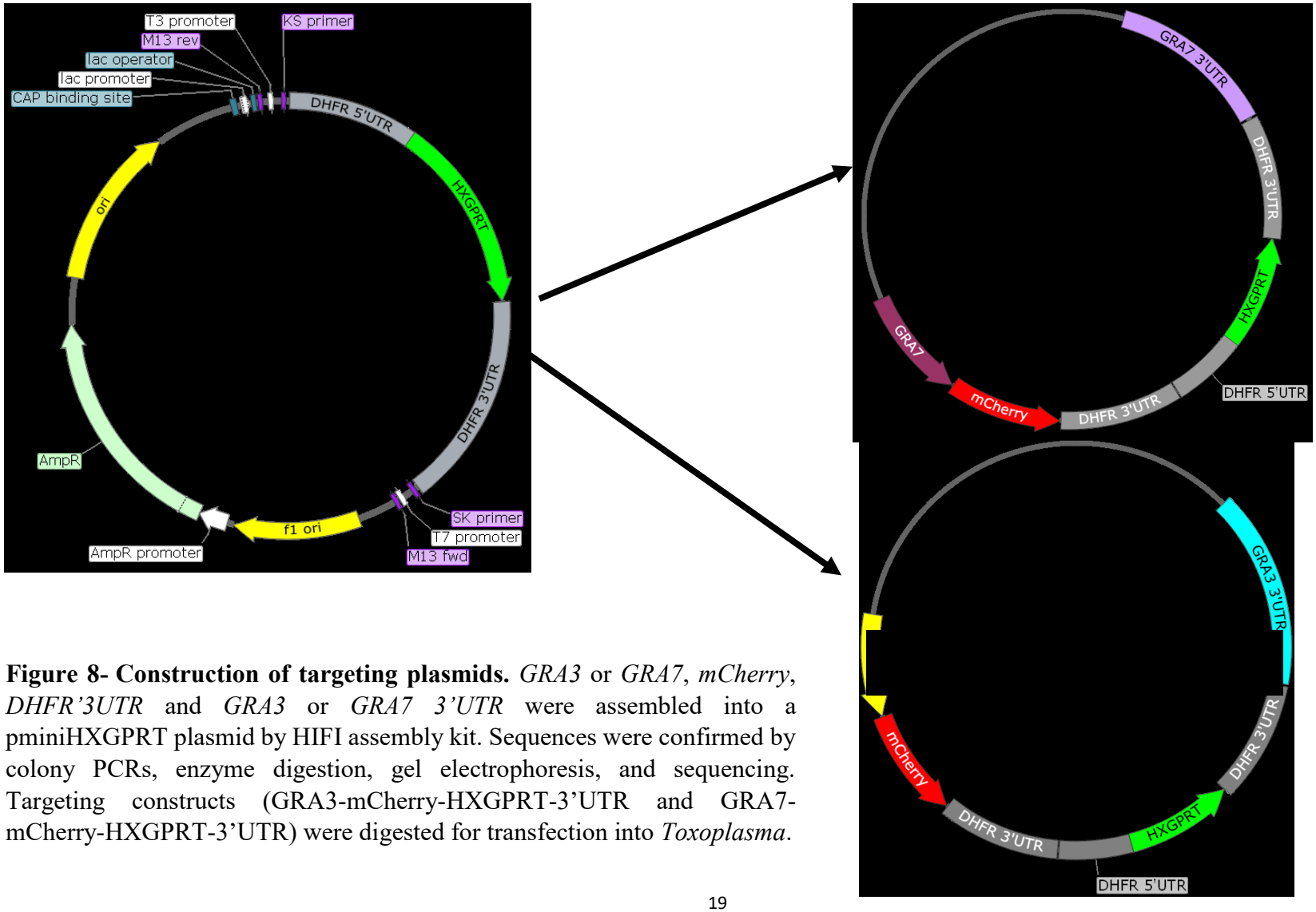

Figure 8- Construction of targeting plasmids. *GRA3* or *GRA7*, *mCherry*, *DHFR'3UTR* and *GRA3* or *GRA7 3'UTR* were assembled into a pminiHXGPRT plasmid by HIFI assembly kit. Sequences were confirmed by colony PCRs, enzyme digestion, gel electrophoresis, and sequencing. Targeting constructs (GRA3-mCherry-HXGPRT-3'UTR and GRA7-mCherry-HXGPRT-3'UTR) were digested for transfection into *Toxoplasma*.

Ipswich, MA), extracted with a QIAquick Gel Extraction Kit (Hilden, Germany) and confirmed by DNA sequencing.

D. Generation of *GRA3-mCherry* and *GRA7-mCherry* strains

To generate *GRA3-mCherry* or *GRA7-mCherry* parasite strains, freshly egressed *ΔKu80Δhxgprt* parasites were collected, pelleted and resuspended in Cytomix buffer (2mM EDTA,120mM KCL, 0.15mM $CaCl_2$, 10mM K_2HPO_4/KH_2PO_4, 25mM HEPES, 5mM $MgCl_2.6H_2O$; pH7.6). *ΔKu80Δhxgprt* parasites were transfected by electroporation (setting: 1.5KV, 25Ohms resistance, 25µF capacitance, time constant of 0.3-0.7µs) with CRISPR plasmids (30µg) containing either GRA3 gRNA or GRA7 gRNA and the corresponding digested targeting plasmids (30µg). After overnight incubation with HFF cells, transfectants were placed under selection with 25µg/ml mycophenolic acid, 59µg/ml xanthine and 0.1N HCl. After 2-3 days of drug selection, transfectants were plated for single clones in 96-well plates. Individual clones were screened for GRA3-mCherry or GRA7-mCherry signal using a Nikon T200 microscope equipped with a 40X objective. For each strain, two single clonal populations were obtained.

E. Confirmation of mCherry insertion into the parasite genome

To confirm if the inserted targeting construct is in the correct location in the genome of GRA3-mCherry and GRA7-mCherry strains, PCR was carried out using Expand High Fidelity PCR kit (Roche, Switzerland). Primers used for PCR were designed using NCBI Primer Designing Tool (https://www.ncbi.nlm.nih.gov/tools/primer-blast/). All primers used are listed in Table II. Primers outside *GRA3* or *GRA7* and within the *mCherry* sequence region were used to detect the insertion of *mCherry* at the 3'end of *GRA3* or

GRA7. Primers within the *HXGPRT* and outside the *3'UTR* of *GRA3* or *GRA7* were used to detect the presence of *HXGPRT*. Genomic DNA of *GRA3-mCherry*, *GRA7-mCherry* and parental strains were extracted using GenElute Mammalian Genomic DNA Miniprep Kit.

PCR amplification was in a 0.2ml PCR tube consisting 50uL of PCR reaction mixture (150ng DNA template, 1X expand buffer with 15mM $MgCl_2$, 200µM dNTPs, 300nM of primers, 0.75µl High Fidelity enzyme and H_2O) and was run on a C1000 Touch Thermal Cycler (Bio-Rad Laboratories, Hercules, CA). The thermal cycle was programmed for 2 min at 94 °C for initial denaturation, followed by 10 cycles of 15 s at 94 °C for denaturation, 30 s at corresponding Tm for annealing, 2.5 min at 72 °C for extension, Then the thermal cycle started another 20 cycles (+5 s/cycle) of 15 s at 94°C for denaturation, 30 s at corresponding Tm for annealing, 2.5 min at 72 °C for extension, and ended with 7 min at 72 °C for the final extension. PCR products and the size marker (1 kb DNA ladder; New England Biolabs, Ipswich, MA) were separated by electrophoresis at 75 V for 1.5 hours in a 1% agarose gel in 1 x TBE buffer (10.8g Tris,5.5g Boric acid, and 0.5M Na_2EDTA in H_2O). The electrophoresis gel was soaked in 0.5µg/ml ethidium bromide for 20 minutes and then examined in UV light.

F. Plaque assays

HFF cells were grown in 6-well plates until confluent. Freshly egressed *GRA3-mCherry, GRA7-mCherry* and *ΔKu80Δhxgprt* parasites were counted with a hemocytometer and 100 parasites were added per well of 6-well plates. The plates were incubated at 37°C in 5% CO2 for 6 days. The cells were then fixed in 100% of ethanol for

5 min and stained in a crystal violet solution (1% of ammonium oxalate and 10% of crystal violet in 100% ethanol) for 5 min. The plates were scanned using a ScanWizard 5 scanner (Microtek, Santa Fe Springs, CA). The area of each plaque was measured using Volocity software (PerkinElmer, Waltham, MA) using an ROI tool. The mean area and SD of the plaques were calculated from three independent experiments, and p values were calculated using the paired T test in Prism GraphPad (La Jolla, CA).

G. Immunoblotting

Freshly egressed parasites of *GRA3-mCherry*, *GRA7-mCherry* and *ΔKu80Δhxgprt* strains were collected from one well of a 6-well plate, pelleted and washed with 1ml of 1X PBS. Parasites were then resuspended into 24µl RIPA butter (10mM Tris-Cl, 1mM EDTA, 1% Triton X-100, 0.1% $C_{24}H_{39}NaO_4$, 0.1% SDS, 140mM NaCl and 1mM PMSF), 6ul 5X sample buffer (0.25M Tris-HCl, 0.5M DTT, 10% SDS, 50% glycerol, 0.5% Bromophenol Blue) and 0.6µl Beta-mercaptoethanol and boiled for 5 min. Cell lysates (10µl) were separated by SDS-PAGE and transferred to a polyvinylidene fluoride (PVDF) membrane (Millipore, Bedford, MA). The membrane was blocked in blocking buffer (10% milk in 1X PBS) for 60 min, and then incubated with either mouse anti-GRA3 (1:8000), or rabbit anti-GRA7 (1:5000) antibodies for 60 min, or rabbit anti-DsRed in 5% milk/PBST(1X PBS and 0.1% Tween 20) for overnight. The membrane was then washed with PBST for three 5-min washes. Next, the membrane was incubated with horseradish peroxidase-conjugated donkey anti-rabbit IgG antibody or goat anti-mouse IgG antibody (1:10,000 in 5% milk/PBST) for 1 hour, followed by three 5-min washes before detection by chemiluminescence (Bio-Rad Laboratories, Hercules, CA).

H. Immunofluorescence and fixed cell microscopy

To perform immunofluorescence assays (IFA), strains of freshly egressed *Toxoplasma* were used to infect HFFs grown on coverslips for 30 min, followed by cascade washes with 1X PBS to remove non-evading extracellular parasites. After a 20-hour incubation, coverslips were fixed with fixative solution (4% formaldehyde and 0.02% glutaraldehyde in PBS) for 15 min, washed with PBS and permeabilized with 0.3% Triton X-100/PBS for 5 min. The coverslips were then washed with 1X PBS and blocked in blocking buffer (3% BSA/PBS) for 1 hour, followed by incubation in primary antibody diluted 1:600 in 3%BSA/PBS for 1 hour and later three 5-min PBS washes. The samples were incubated with secondary antibody diluted 1:2000 in 3% BSA/PBS for 1 hour, followed by three 5-min PBS washes. Nucleus of HFF and *Toxoplasma* was detected by incubating coverslips in 1mg/ml DAPI diluted 1:1000 in PBS for 5 min. Coverslips were mounted with ProLong Diamond Antifade Mountant (Life Technologies, Carlsbad, CA). Cells were viewed with a Zeiss AxioImager M2 fluorescence microscope equipped with an oil-immersion Zeiss plan Apo 100x/NA 1.4 objective and a Hamamatsu ORCA-R2 camera. Optical z-sections with 0.2µm spacing were acquired using Volocity 6.3.1 acquisition module (Perkin Elmer, Waltham, MA).

I. Live cell imaging

HFF or VERO cells stably expressing GFP-Rab11A were plated into wells of a 24-well microscopy plate (ibidi GmbH, Martinsried, Germany) and infected with freshly egressed GRA3-mCherry expressing parasites for 24 hours. Cells were viewed using a DeltaVision RT microscope system (Applied Precision, Issaquah, WA) equipped with a 60x oil immersion objective (NA 1.42), a humidified chamber with temperature (37°C) and CO_2 (5%) control, and a Scientific CMOS camera. Live time-lapse images were captured as z-stacks with a step size of 0.2µm and deconvolved (Softworx, Applied Precision). Image analysis and preparation was performed using Fiji Image J (Schindelin et al., 2012).

J. Image Analysis

For intracellular growth assay, 100 of PV were randomly chosen for each strain. The mean area and SD of the parasite per PV were calculated from three independent experiments, and p values were calculated using the paired T test in Prism GraphPad.

Images from fixed cell microscopy were deconvolved with an iterative restoration algorithm using calculated point spread functions, adjusted brightness and contrast, and cropped through Volocity software. To measure the level of colocalization using Volocity, Pearson's correlation coefficients (PCCs) were calculated along with a positive product of the difference of the means (PDM).

Table I-Plasmids used for generating *GRA3-mCherry* and *GRA7-mCherry* strains.

Plasmid	Used for
pSAG1::CAS9-U6::sgUPRT	Constructing mutagenized CRISPR/Cas9 plasmids targeting *GRA3 gRNA* or *GRA7 gRNA*
pSAG1::CAS9-U6::GRA3 gRNA	CRISPR plasmid targeting *GRA3 gRNA*
pSAG1::CAS9-U6::GRA7 gRNA	CRISPR plasmid targeting *GRA7 gRNA*
pTUB-GRA3-YFP	Amplifying *GRA3*
pmCherry-C1	Amplifying *mCherry*
pminiHXGPRT	Constructing targeting constructs
GRA3-mCherry-HXGPRT-GRA3 3'UTR	Generating GRA3-mCherry *Toxoplasma* strain
GRA7-mCherry-HXGPRT-GRA7 3'UTR	Generating GRA7-mCherry *Toxoplasma* strain

Table II-Primers used for generating *GRA3-mCherry* and *GRA7-mCherry* strains.

Primer name	Primer Sequence	Used for
F.sibley	GAGCCAAGGGGGAAACCTTCGAACTCTCGAA	DNA Sequencing confirmation for plasmids pSAG1::CAS9-U6::GRA3 gRNA and pSAG1::CAS9-U6::GRA7 gRNA
oJR110	GGAACAAAAGCTGGTACCATGGACCGTACCATATGTC	Forward primer to amplify *GRA3* from plasmid pTUB GRA3-YFP
oJR111	ATGGGCCCTTTCTTGGAGGCTTTGTC	Reverse primer to amplify *GRA3* from plasmid pTUB-GRA3-YFP
oJR112	TCCAAGAAAGGGCCCATGGTGAGCAAGGGCGAGG	Forward primer to amplify *mCherry* from plasmid pmCherry-C1 for making GRA3-mCherry-HXGPRT-GRA3 3'UTR plasmid
oJR113	TCGATACCGTCGACCTCGAGCTACTTGTACAGCTCGTCCATG	Reverse primer to amplify *mCherry* from plasmid pmCherry-C1 for making GRA3-mCherry-HXGPRT-GRA3 3'UTR plasmid
oJR114	TTCATGAGTTGTTTTAGAGCTAGAAATAGC	Forward primer to replace *sg UPRT* to *GRA3 gRNA* in plasmid pSAG1::CAS9-U6::sgUPRT
oJR115	GGGTTGCCTCAACTTGACATCCCCATTTAC	Reverse primer to replace *sg UPRT* to *GRA3 gRNA* in plasmid pSAG1::CAS9-U6::sgUPRT
oJR122	GGCGAAGATGGTTTTAGAGCTAGAAATAGC	Forward primer to replace *sg UPRT* to *GRA7 gRNA* in plasmid pSAG1::CAS9-U6::sgUPRT

oJR123	TGATTCAGGCAACTTGACATCCCCATTTAC	Reverse primer to replace *sg UPRT* to *GRA7 gRNA* in plasmid pSAG1::CAS9-U6::sgUPRT
oJR126	GTGACACCGCGGTGGAGGGGGATCCAGTAGGAGCTCGAGGAC AG	Forward primer to amplify *GRA7 3'UTR* from *Toxoplasma* genomic DNA; also used for colony PCR to confirm the presence of *GRA7 3'UTR*
oJR127	CCACCGCGGTGGCGGCCGCTCTAGAAGTAGAGCAAGAAACGCA AG	Reverse primer to amplify *GRA7 3'UTR* from *Toxoplasma* genomic DNA; also used for colony PCR to confirm the presence of *GRA7 3'UTR*
oJR130	CACTAAAGGGAACAAAAGCTGGTACCATGGCC CGACACGCAATTTTTTCCGC	Forward primer to amplify *GRA7* from *Toxoplasma* genomic DNA; also used for colony PCR to confirm the presence of *GRA7*
oJR131	CCTTGCTCACCATGGGCCCCTGGCGGGCATC	Reverse primer to amplify *GRA7* from *Toxoplasma* genomic DNA; also used for colony PCR to confirm the presence of *GRA7*
oJR132	CCGCCAGGGGCCCATGGTGAGCAAGGGCGAG	Forward primer to amplify *mCherry* from pmCherry-C1 to create GRA7-mCherry-HXGPRT-GRA7 3'UTR
oJR133	CAGCTTCTGTGGGCTCGAGCTACTTGTACAGCTC	Reverse primer to amplify *mCherry* from pmCherry-C1 to create GRA7-mCherry-HXGPRT-GRA7 3'UTR
oJR134	CAAGTAGCTCGAGCCCACAGAAGCTGCCCGT	Forward primer to amplify *DHFR 3'UTR* from pmini-HXGPRT plasmid to create GRA7-mCherry-HXGPRT-GRA7 3'UTR

oJR135	TGAATGCAAGGTTTCGTGCTGATCAAGCTTGCGGTGTCACTGTAGCCTG	Reverse primer to amplify *DHFR 3'UTR* from pmini-HXGPRT plasmid to create GRA7-mCherry-HXGPRT-GRA7 3'UTR; also used as the reverse primer to amplify *DHFR 3'UTR* to create GRA3-mCherry-HXGPRT-GRA3 3'UTR and colony confirmation
oJR136	GGACGAGCTGTACAAGTAGCTCGAGACCCTGCATAGCCCACAG	Forward primer to amplify *DHFR 3'UTR* from pmini-HXGPRT plasmid to create GRA3-mCherry-HXGPRT-GRA3 3'UTR and colony PCR confirmation
oJR137	GTGACACCGCGGTGGAGGGGGATCCCCTGAAACATTCGTTGACG	Forward primer to amplify *GRA3 3'UTR* from *Toxoplasma* genomic DNA to create GRA3-mCherry-HXGPRT-GRA3 3'UTR; also used for colony PCR to confirm the presence of *GRA3 3'UTR*
oJR138	CCACCGCGGTGGCGGCCGCTCTAGATTTGCGCGATGTCGATGTAC	Forward primer to amplify *GRA3 3'UTR* from *Toxoplasma* genomic DNA; also used for colony PCR to confirm the presence of *GRA3 3'UTR*

oJR139	GCTCACGCAGAGGCAATACT	Forward primer to amplify *GRA3* to *mCherry* in the genome of GRA3-mCherry strain; test location in genome
oJR140	TGGCCTTGTAGGTGGTCTTG	Reverse primer to amplify *GRA3* to *mCherry* in the genome of GRA3-mCherry strain; test location in genome
oJR141	CGGTCCCAAGTCGATGAGAAT	Forward primer to amplify *HXGPRT* to *GRA3 3′ UTR*; test whether *GRA3-mCherry* was inserted in the correct location in the genome
oJR142	CGCGTCGAGTAACCAGTGAG	Forward primer to amplify *GRA3* to *GRA3 3'UTR* the genome of GRA3-mCherry strain; test location in genome
oJR143	GCATGGTTGCAAAGTCCTGC	Reverse primer to amplify *GRA3* to *GRA3 3'UT* the genome of GRA3-mCherry strain; also pair with oJR141 as the reverse primer to amplify *HXGPRT* to *GRA3 3′ UTR*
oJR144	TCGACGTCTTTGGAACGTGT	Forward primer to amplify *GRA7* to *mCherry* in the genome of GRA7-mCherry strain; test location in genome
oJR145	CAAGTAGTCGGGGATGTCGG	Reverse primer to amplify *GRA7* to *mCherry* in the genome of GRA7-mCherry strain; test location in genome

oJR146	CAGAACGACAACAGCACAGG	Forward primer to amplify *HXGPRT* to *GRA7 3′ UTR* in the genome of GRA7-mCherry strain; test location in genome
oJR150	TCCATTCGTCGCTACCGTTG	Forward primer to amplify *GRA7* to *GRA7 3′ UTR* in the genome of GRA7-mCherry strain; test location in genome
oJR151	CGGTAACGCGCATAAAACGA	Reverse primer to amplify GRA7 to GRA7 3' UTR in the genome of GRA7-mCherry
R230 5’HXGPRT	ACGGAAAGTGCTTACATCGAACACGGTTATCAAAC	Reverse primer to amplify HXGPRT region

3. RESULTS:

A. Generation of GRA3-mCherry and GRA7-mCherry expressing strains using CRISPR/Cas9

To label GRA3 and GRA7, we used a CRISPR-Cas9 system to insert mCherry into the genome. First, we created an RNA-guided Cas9 plasmid to target either GRA3 or GRA7 in the genome. The guide RNA was designed using Eukaryotic Pathogen CRISPR guide RNA/DNA Design Tool (http://grna.ctegd.uga.edu/) and E-CRISPR (http://www.e-crisp.org/E-CRISP/) websites, and were chosen that were located at the 3' end of *GRA3* or *GRA7*. The Cas9 protein/ gRNA complex specifically targets *GRA3* or *GRA7* in the genome of *Toxoplasma* and creates a double-stranded break (Figures 9 and 10). Second, we created the targeting constructs containing *GRA3* or *GRA7*, *mCherry*, *HXGPRT*, and *GRA3 3'UTR* or *GRA7 3'UTR*. The *mCherry* was inserted on the C-terminus of *GRA3* or *GRA7* because these proteins contain an N-terminual secretory signal sequence. *GRA3* or *GRA7* and its corresponding *3'UTR* sequence on the targeting construct are used for homologous recombination to repair the DSB mediated by Cas9 nuclease (Figures 9 and 10). *HXGPRT* (hypoxanthine-xanthine-guanine phosphoribosyl transferase) is involved in the Purine metabolism pathway (IMP) of *T. gondii*. Strains expressing HXGPRT activity can be selected in mycophenolic acid and xanthine (Pfefferkorn and Borotz, 1994). The parental *Toxoplasma* strain we used is *Δku80Δhxgprt,* in which the Ku80 mutation disrupts the parasite's NHEJ pathway, resulting in a switch to homologous recombination (Huynh and Carruthers, 2009). Transfected parasites expressing either GRA3-mCherry (Figure

11A) or GRA7-mCherry (Figure 11B) were detected under the microscope and selected for single clones.

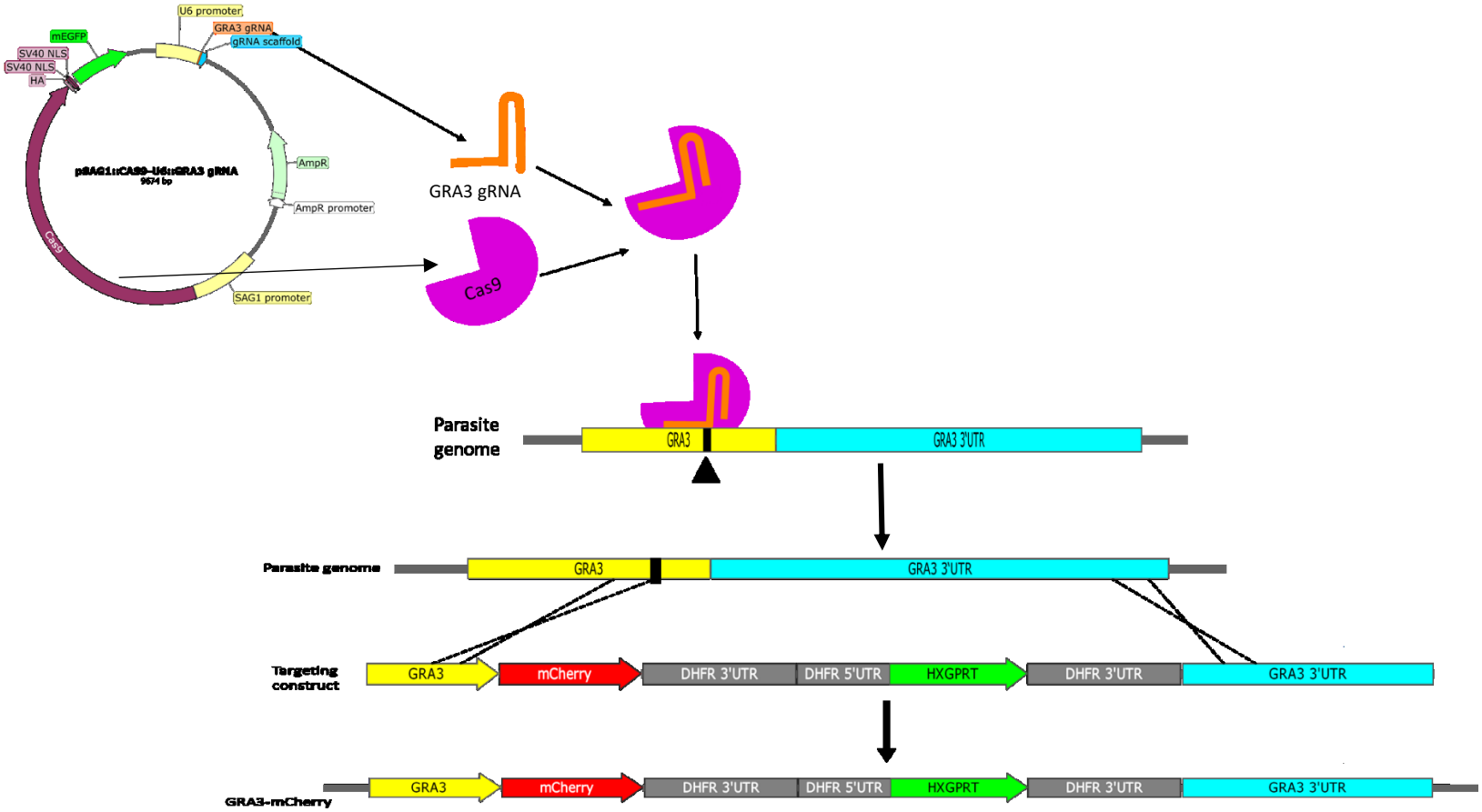

Figure 9-Generation of the GRA3-mCherry expressing strain. The Cas9 protein and GRA3 gRNA are expressed from the same plasmid and bind together to form a complex. The Cas9 protein/GRA3 gRNA complex specifically targets *GRA3* in the genome of *Toxoplasma*, and creates a double-stranded break (indicated with black triangle). The targeting construct was integrated into the parasite genome through homologous recombination to repair the Cas9-induced double-stranded break. The plasmid map was generated using SnapGene.

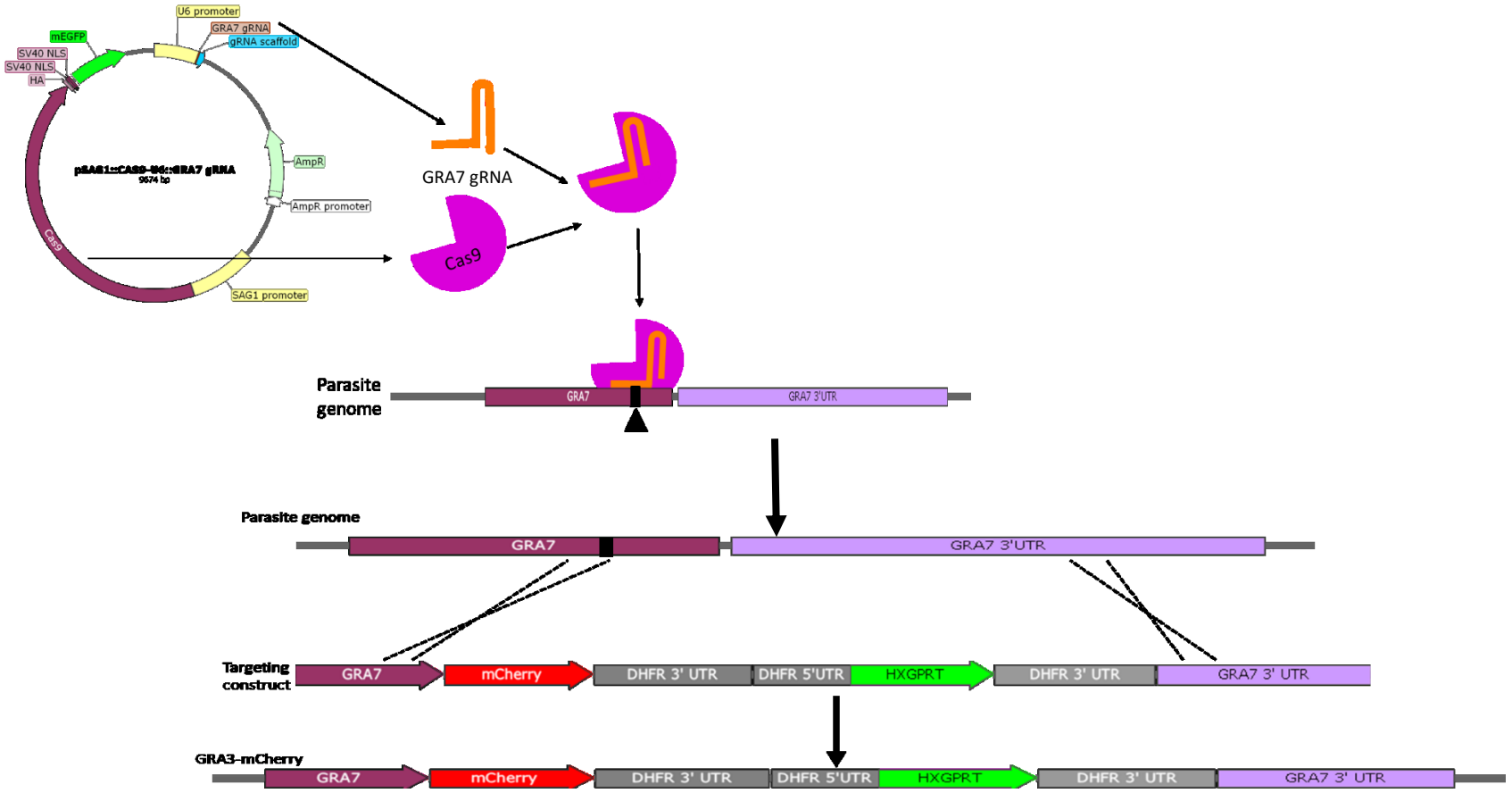

Figure 10-Generation of the GRA7-mCherry expressing strain. The Cas9 protein and GRA7 gRNA are expressed from the same plasmid and bind together to form a complex. The Cas9 protein/GRA7 gRNA complex specifically targets *GRA7* in the genome of *Toxoplasma* and creates a double-stranded break (indicated with black triangle). The targeting construct was integrated into the parasite genome through homologous recombination to repair the Cas9-induced double-stranded break. The plasmid map was generated using SnapGene.

A

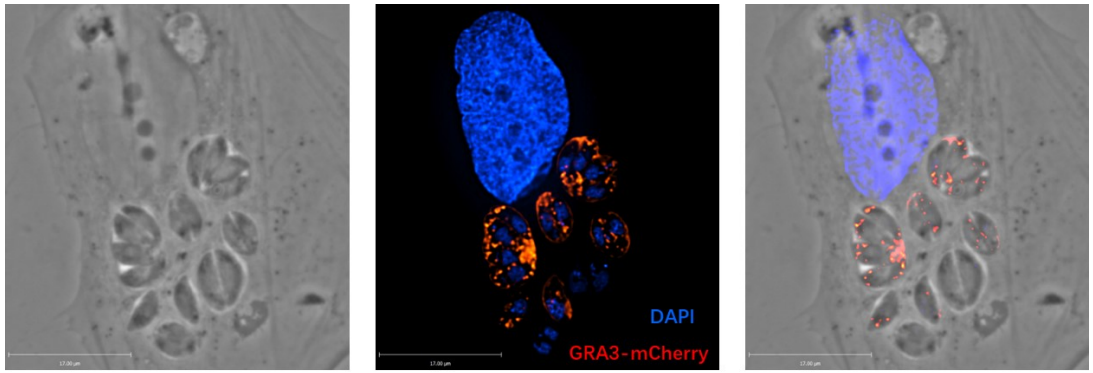

B

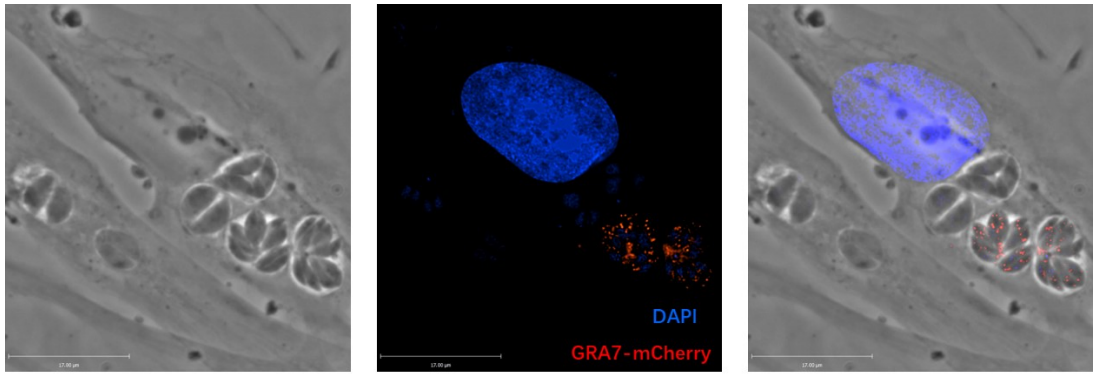

Figure 11-Transfected parasites expressing either GRA3-mCherry or GRA7-mCherry. The targeting constructs (GRA3-mCherry-HXGPRT-GRA3 3'UTR or GRA7-mCherry-HXGPRT-GRA7 3'UTR) were digested and transfected, along with a plasmid expressing Cas9 and the appropriate gRNA, into the *Δku80Δhxgprt* parasite strain. After transfection, the presence of GRA3-mCherry (A) and GRA7-mCherry (B) was detected by infecting HFF cells with the transfected parasites for 24 hours. Nuclei were stained with DAPI (blue). Phase (left), fluorescent image (middle), merge (right). Images were deconvoluted and processed using Volocity Software.

B. Confirmation of the genomic location of the mCherry targeting construct

The insertion of *mCherry* into the *GRA3* or *GRA7* locus was verified by PCR. Primers were designed to amplify a 5' region of the *GRA3* or *GRA7* gene (outside of the region used in the targeting construct) within the *mCherry* gene (Figures 12A and 13A). Likewise, primers were designed to amplify a region outside of the *GRA3* or *GRA7* 3' *UTR* to within the *HXGPRT* gene No bands were amplified from genomic preparations of *Δku80Δhxgprt* parasites, indicating the absence of the targeting constructs in the parental genome (Figures 12B, 12C, 13B and 13C). PCR products of the expected size were amplified from the two clonal populations expressing GRA3-mCherry - 1334bp (*GRA3 5' UTR* to *mCherry)* and 2359bp (*HXGPRT* to the *GRA3 3'UTR*), indicating that the targeting construct is correctly integrated in the parasite genome (Figure 12B and 12C). Similar results were found for the GRA7-mCherry expressing strains (Figure 13B and 13C). Overall, our results show that the targeting construct is specifically inserted at the 3' end of the *GRA3* and *GRA7 genes* in the parasite genome.

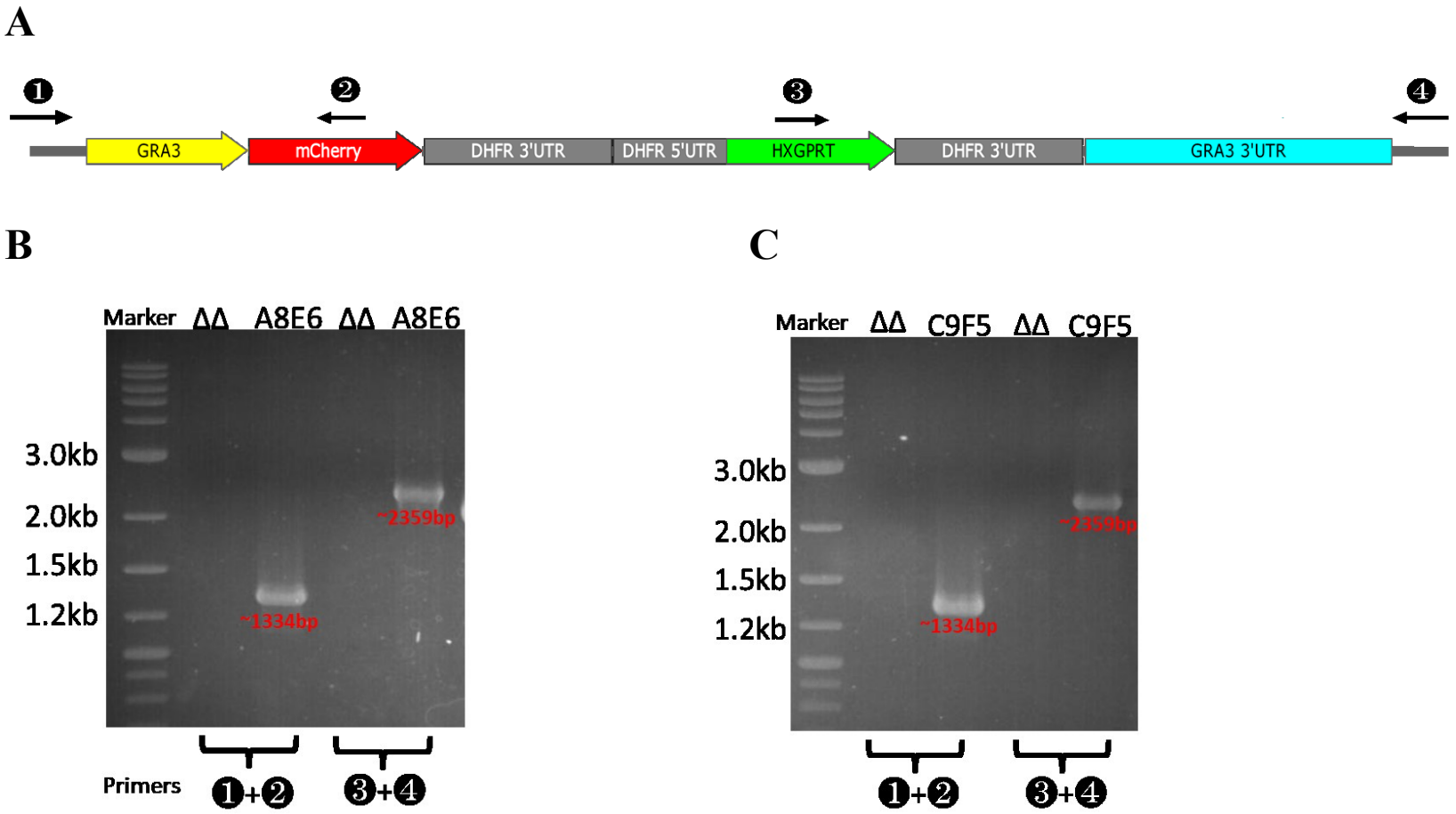

Figure 12-Confirmation of the insertion of *mCherry* at the 3' end of *GRA3* in the genome. A) Schematic representation of the targeting construct integrated into the *GRA3* genomic locus. Primers used to confirm the insertion of the targeting construct by PCR are shown. B) and C) PCR of *Δku80Δhxgprt* and two GRA3-mCherry clonal populations. The P1/P2 primers were used to verify the presence of *mCherry* while the P3/P4 primers verified the presence of *HXGPRT*. ΔΔ: *Δku80Δhxgprt* strain. A8E6 and C9F5: 2 clonal populations expressing *GRA3-mCherry*. Primer 1: OJR139. Primer 2: OJR 140. Primer 3: OJR141. Primer 4: OJR143.

A

B

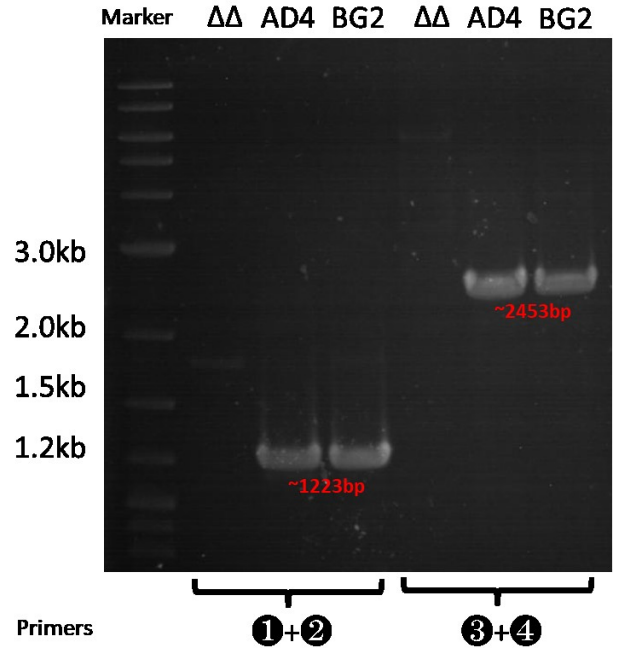

Figure 13-Confirmation of the insertion of *mCherry* at the 3' end of the *GRA7* gene in the genome. A) Schematic representation of the targeting construct integrated into the *GRA7* genomic locus. Primers used to confirm the insertion of the targeting construct by PCR are shown. B) and C) PCR of *Δku80Δhxgprt* and two clonal populations expressing GRA7-mCherry. The P1/P2 primers were used to verify the presence of *mCherry* while the P3/P4 primers verified the presence of *HXGPRT*. ΔΔ: *Δku80Δhxgprt* strain. AD4 and BG2: 2 clonal populations expressing *GRA7-mCherry*. Primer 1: OJR144. Primer 2: OJR 145. Primer 3: OJR146. Primer 4: OJR151.

C. Detection of GRA3-mCherry and GRA7-mCherry proteins by immunoblotting

Expression of GRA3-mCherry and GRA7-mCherry was detected by Western blot using anti-GRA3, anti-GRA7 and anti-mCherry antibodies. Based on the primary sequence, the predicted molecular weight of GRA3 is 24.25 kDa and of GRA7 is 25.86 kDa. The predicted molecular weight of mCherry is ~27 kDa. Expression of endogenous GRA3 (~24 kDa) was detected in the *Δku80Δhxgprt* strain (Figure 14A). In the two clonal GRA3-mCherry expressing strains, bands at ~51 kDa for GRA3-mCherry were detected either with anti-GRA3 antibody (Figure 14A) or by anti-mCherry antibody (Figure 14B), indicating the expression of GRA3-mCherry. Probing lysates from the *Δku80Δhxgprt* strain with antibodies against mCherry did not detect any bands, confirming the lack of mCherry in the parental strain. Additional bands with molecular weights between 25 kDa to 37 kDa were also detected in the GRA3-mCherry expressing strains. Those bands most likely represent degraded peptides.

GRA7 was detected as a ~26 kDa band in *Δku80Δhxgprt.* GRA7-mCherry (~53 kDa) was detected in the two clonal GRA7-mCherry expressing strains either by anti-GRA7 antibody (Figure 15A) or anti-mCherry antibody (Figure 15B). Several bands lower than GRA7-mCherry (~53 kDa) were also detected in the GRA7-mCherry strains (Figure 15A), indicating the cleavage of the GRA7-mCherry protein. In addition, a band lower than GRA7-mCherry (~53 kDa) was detected in GRA7-mCherry expressing strains by anti-mCherry antibody (Figure 15B), most likely representing cleavage of the GRA7-mCherry protein.

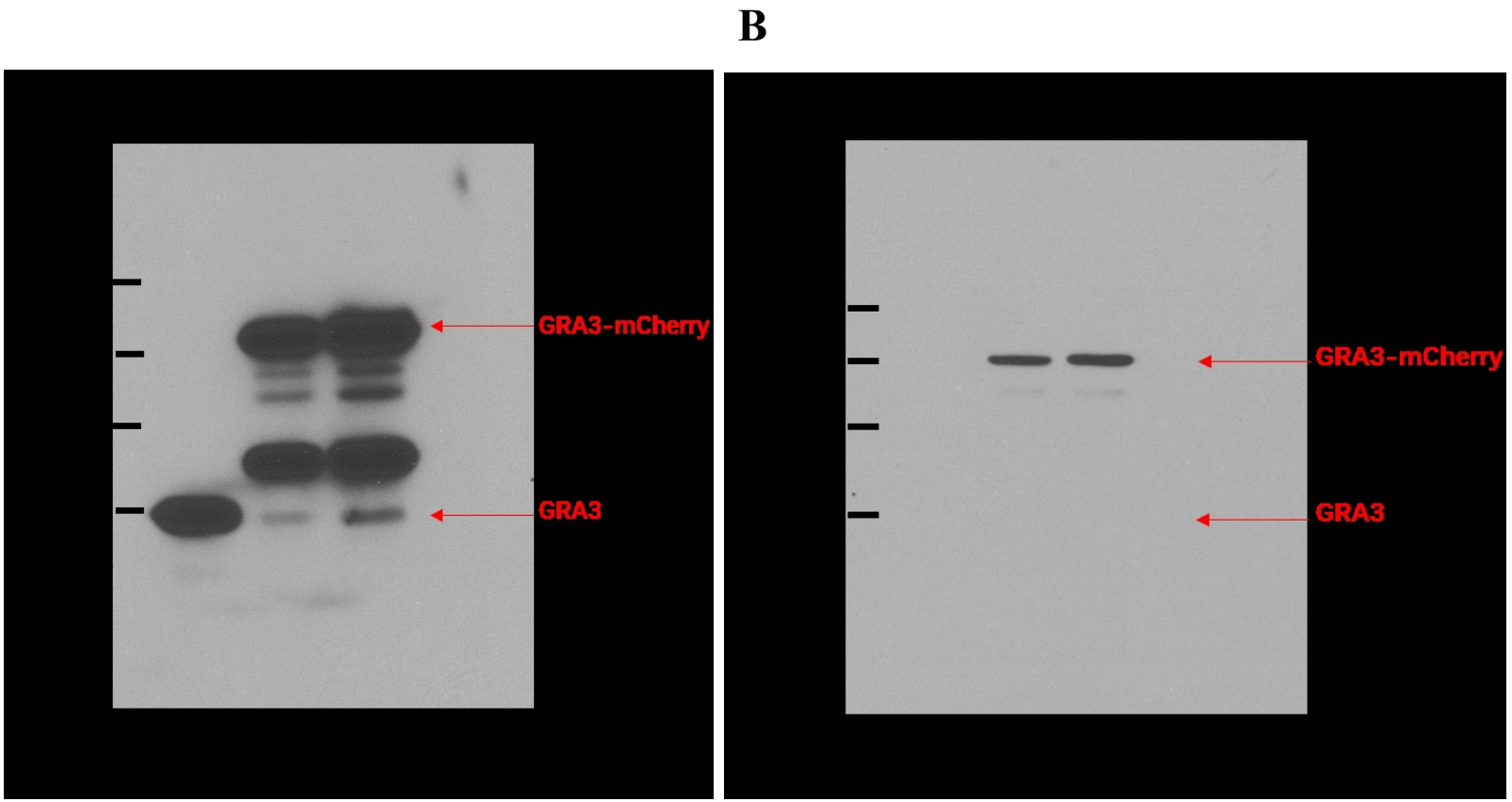

Figure 14-Western blot analysis of GRA3-mCherry. Cell lysates from freshly egressed *ΔKu80Δhxgprt* and two clonal populations of GRA3-mCherry parasites were separated by SDS-PAGE. Blots were incubated with either anti-GRA3 antibody (A) or anti-mCherry antibody (B). Expression of GRA3 protein (24.25KDa) and GRA3-mCherry proteins (50.74KDa) were detected by chemiluminescence. ΔΔ: *Δku80Δhxgprt* strain. A8E6 and C9F5: 2 clonal populations of *GRA3-mCherry* strain. MW indicates the molecular weight markers in kilodaltons.

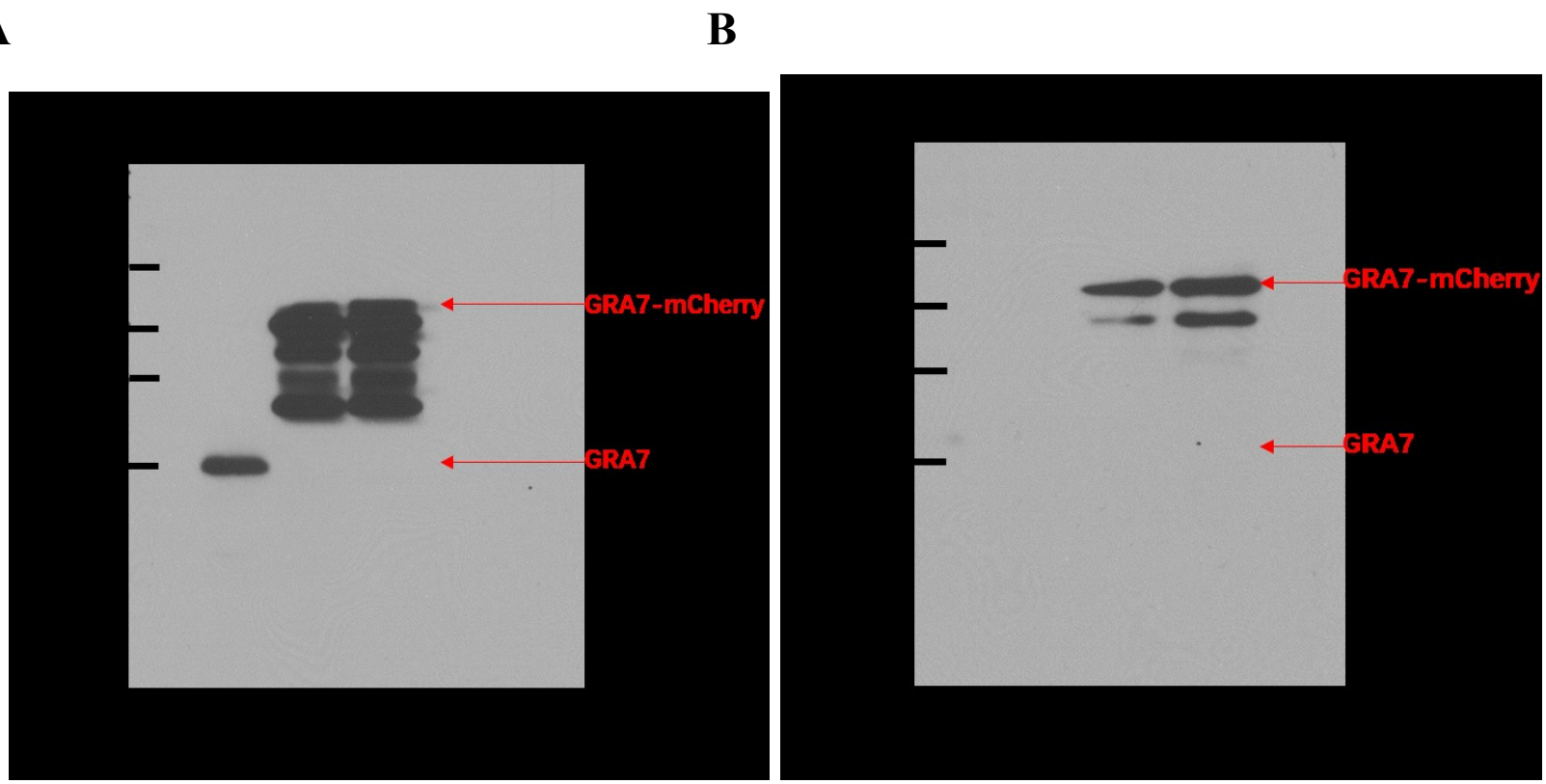

Figure 15-Western blot analysis of GRA7-mCherry. Cell lysates from freshly egressed *ΔKu80Δhxgprt* and two clonal populations of GRA7-mCherry expressing strains were separated by SDS-PAGE. Blots were incubated with either anti-GRA7 antibody (A) or anti-mCherry antibody (B). Expression of GRA3 protein (25.86 KDa) and GRA3-mCherry proteins (52.72KDa) were detected by chemiluminescence. ΔΔ: *Δku80Δhxgprt* strain. AD4 and BG2: 2 clonal populations of *GRA7-mCherry* strain. MW indicates the molecular weight markers in kilodaltons.

D. Localization assays for GRA3-mCherry and GRA7-mCherry

To ascertain that the insertion of mCherry does not interfere with GRA7 or GRA3 localization, immunofluorescence assays were used to compare the localization of GRA3 or GRA7 in the *Δku80Δhxgprt* strain and *GRA3-mCherry* or *GRA7-mCherry* strains using anti-GRA3 or anti-GRA7 antibodies. Results show that the fluorescence signal of GRA3-mCherry was in dense granules, on the PVM and on the IVN, similarly to the signal of anti-GRA3 antibody in the parental strain (Figure 16). This result indicates that the insertion of mCherry did not interfere with the localization of GRA3. Of note, we observed a stronger fluorescence signal for GRA3-mCherry in dense granules and IVN than on the PVM. As the size of the PV increased, the brightness of the GRA3-mCherry signal at the PVM decreased while it increased in dense granules and on the IVN. In contrast, the fluorescence signal of GRA7-mCherry remained mostly in dense granules; the distribution of GRA7-mCherry fluorescence was less at the PVM and IVN as compared to the parental strain, indicating that the insertion of mCherry slightly interfered with the localization of GRA7 (Figure 17).

To confirm that the mCherry signal represents the intact fusion protein GRA3-mCherry or GRA7-mCherry, we also compared the localization of the mCherry with GRA3 or GRA7 immunofluorescence signals. GRA3 and GRA7 were detected with anti-GRA3 and anti-GRA7 antibody, respectively. The level of colocalization of the two signals was measured using a positive product of the difference of the means (PDM). Colocalization results were represented using values of Pearson's correlation coefficient (PCC). When comparing the localization of the mCherry and GRA3 signals in the *GRA3-mCherry* strain, PCC values were found above 0.70 (Figure 18), indicating the level of colocalization

between these two signals was very high. The highest PCC value (0.83) was found for PV containing 2 parasites in the 2-parasite PV (Figure 18). As the size of the PV increased, the strongest colocalization signals were found on the IVN (shown in yellow on Figure 18). On the contrary, when comparing the localization of the mCherry and GRA7 signals in the *GRA7-mCherry* strain, the PCC values were below 0.50 (Figure 19), indicating a low level of colocalization. The overall colocalization signals of mCherry and GRA7 shown in yellow were weak on PVM.

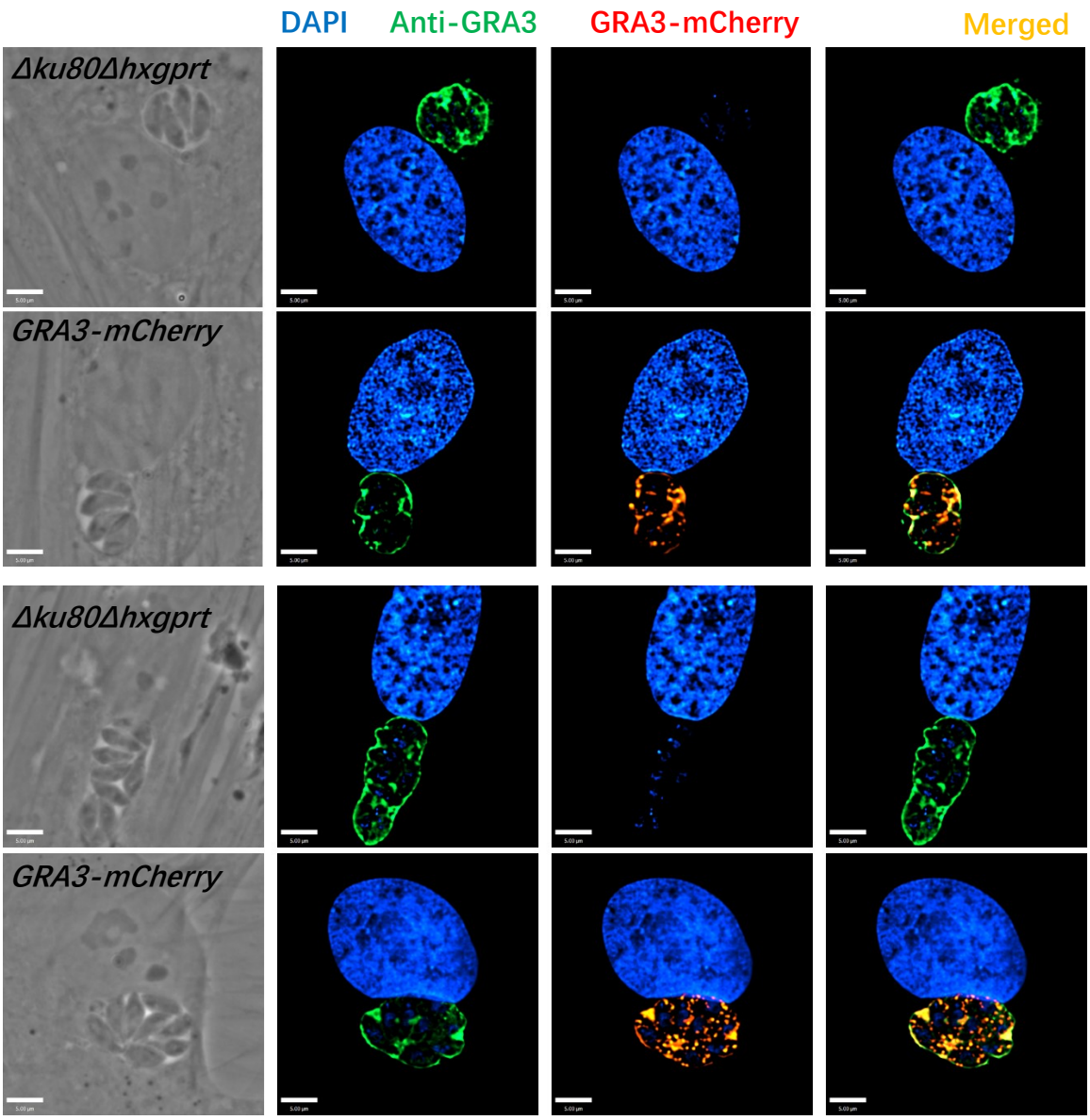

Figure 16- Comparison of GRA3 and GRA3-mCherry localization. HFF were infected with either *Δku80Δhxgprt* or GRA3-mCherry expressing parasites for 24 hours and stained for DAPI (blue) and anti-GRA3 (green). Images were deconvoluted and processed using Volocity Software. Scale bar for each: 5 µ m. Merged: merged channels of anti-GRA3 staining and GRA3-mCherry.

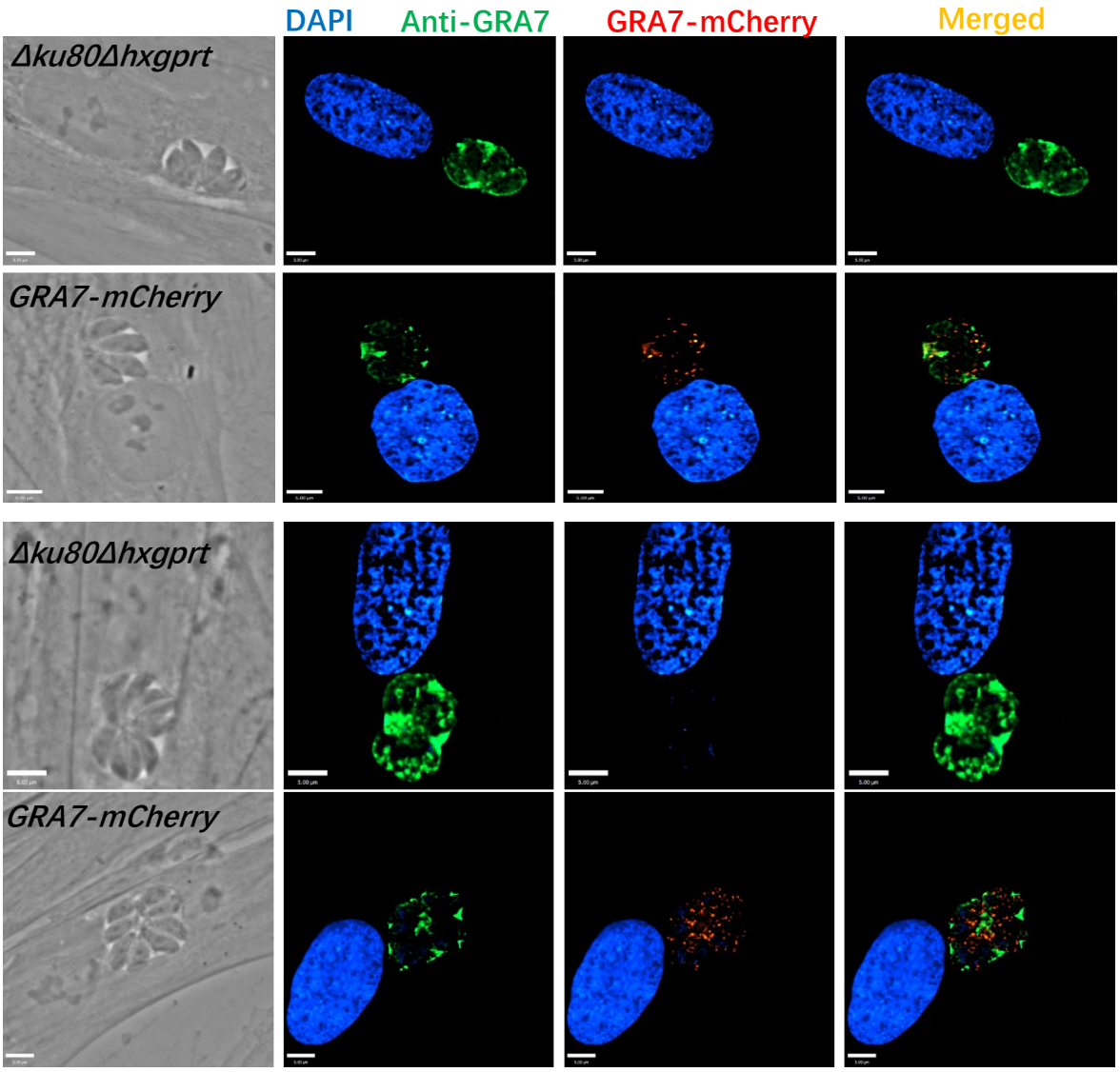

Figure 17- Comparison of GRA7 and GRA7-mCherry localization. HFF were infected with either *Δku80Δhxgprt* or GRA7-mCherry expressing parasites for 24 hours and stained for DAPI (blue) and anti-GRA7 (green). Images were deconvoluted and processed using Volocity Software. Scale bar for each: 5µm. Merged: merged channels of anti-GRA7 staining and GRA7-mCherry.

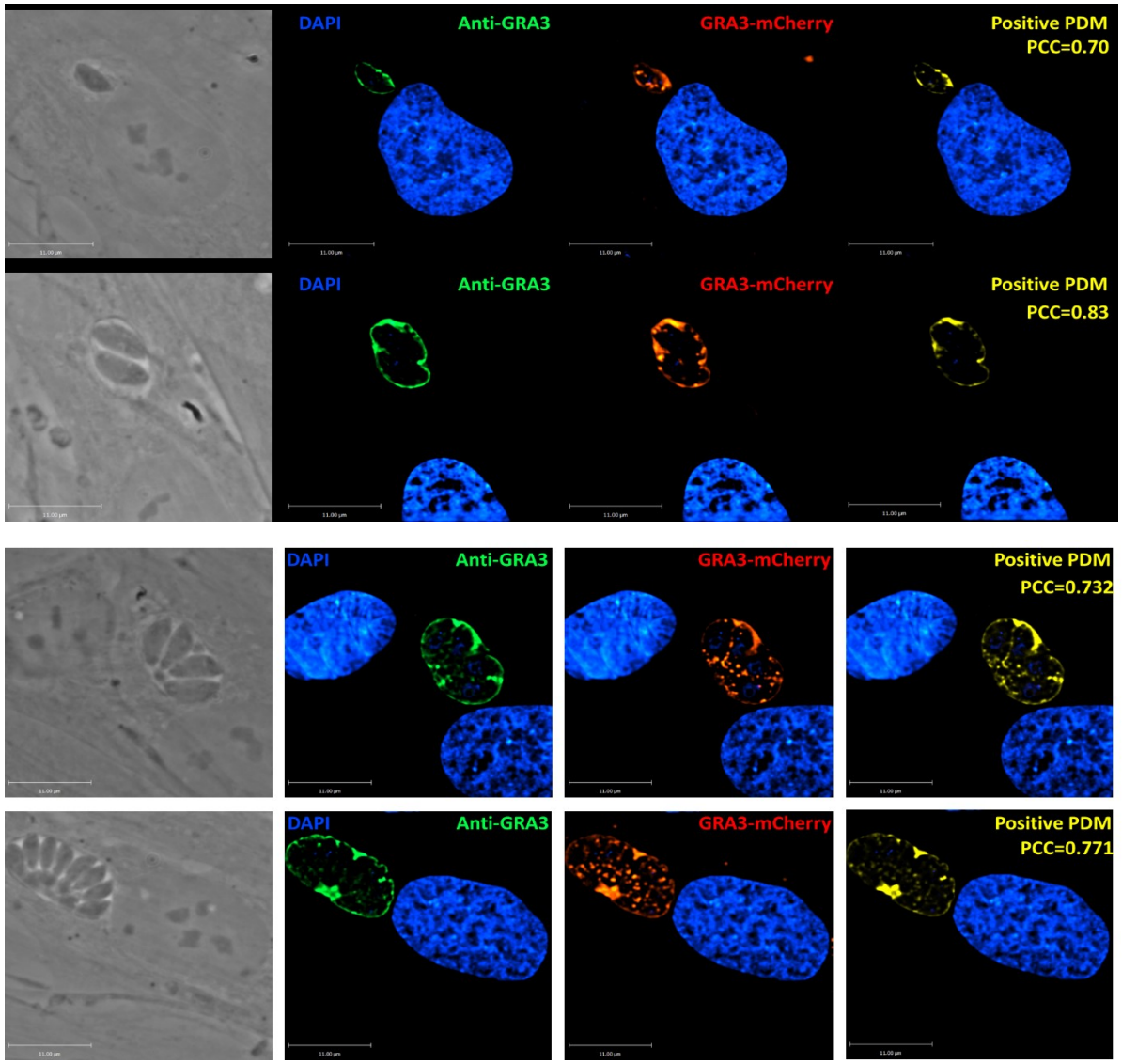

Figure 18-Localization of mCherry and GRA3 in *GRA3-mCherry* strain. HFFs were infected with *GRA3-mCherry* parasites for 24 hours and immunostained for DAPI (blue) and anti-GRA3 (green) antibody. To measure the regions of colocalization, a positive product of the difference of the means (PDM; yellow in panels) for mCherry-tagged GRA3 and antibody-tagged GRA3 was analyzed in Volocity Software. The levels of colocalization were determined using Pearson's correlation coefficient (PCC). Scale bar for each: 11µm.

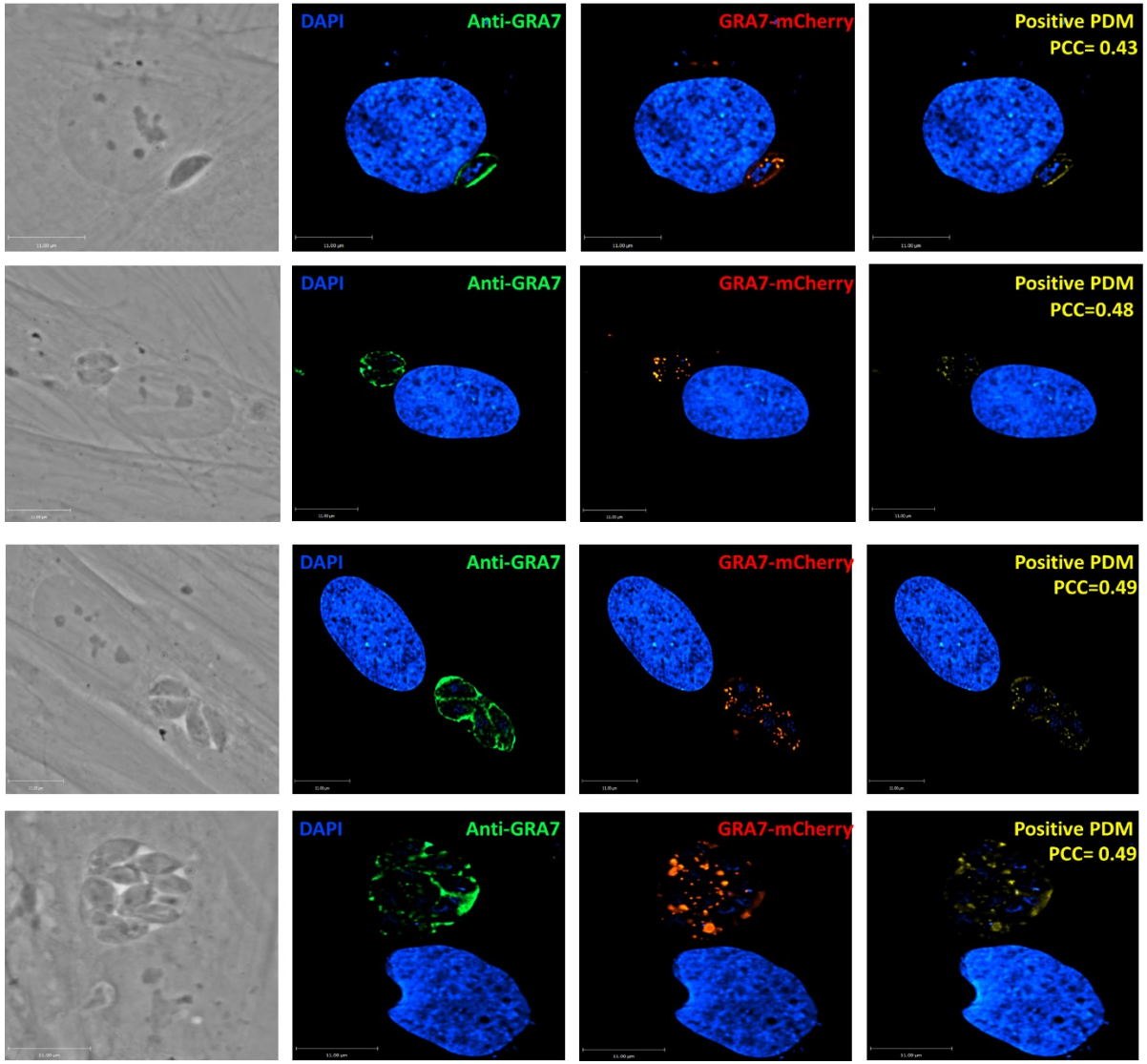

Figure 19-Localization of mCherry and GRA7 in *GRA7-mCherry* strain. HFFs were infected with *GRA7-mCherry* parasites for 24 hours and immunostained for DAPI (blue) and anti-GRA7 (green) antibody. To measure the regions of colocalization, a positive product of the difference of the means (PDM; yellow in panels) for mCherry-tagged GRA7 and antibody-tagged GRA7 was analyzed in Volocity Software. The level of colocalization was determined using Pearson's correlation coefficient (PCC). Scale bar for each: 11µm.

E. Growth Assays for *GRA3-mCherry* and *GRA7-mCherry*

To investigate if the insertion of mCherry at the C-terminus of GRA3 or GRA7 may have disrupted the parasite's development, the growth of the *GRA3-mCherry* and *GRA7-mCherry* strains were compared to that of the parental *Δku80Δhxgprt* strain. Two types of growth assays were performed: the intracellular replication assay and the plaque assay.

Toxoplasma replicates approximately every 8 hours. For the intracellular replication assay, HFF cells were infected with parasites for 30 min, extracellular parasites were eliminated by washing with PBS and then replication was allowed to continue for 20 hours, thus for 2 to 3 cycles of division. The number of parasites per PV were counted, using a microscope, with 100 PVs counted per sample. No difference was noticed in the number of parasites per PV between the parental and *GRA3-mCherry* strains (Figure 20A), or between the parental and *GRA7-mCherry* strains (Figure 20B).

Plaque assays were performed by infecting HFF monolayers grown in 6-well culture plates with 100 parasites for 6 days, allowed several cycles of parasite invasion, replication and egress. After fixation, cells were stained with crystal violet (Figure 21A and 21B). The number of plaques was assessed, and the area of plaques was measured through Volocity software. There was no significant difference in the number of plaques between HFF cells infected with the *Δku80Δhxgprt* strain and either the *GRA3-mCherry* or *GRA7-mCherry* strains (Figure 21C and 21D). Comparing the plaque areas of the *Δku80Δhxgprt* strain with either the *GRA3-mCherry* or *GRA7-mCherry* strains showed no significant differences as well (Figure 21 E and 21F).

In summary, results from our growth assays indicate that tagging GRA3 or GRA7 at the C-terminus with mCherry did not affect parasite growth.

A

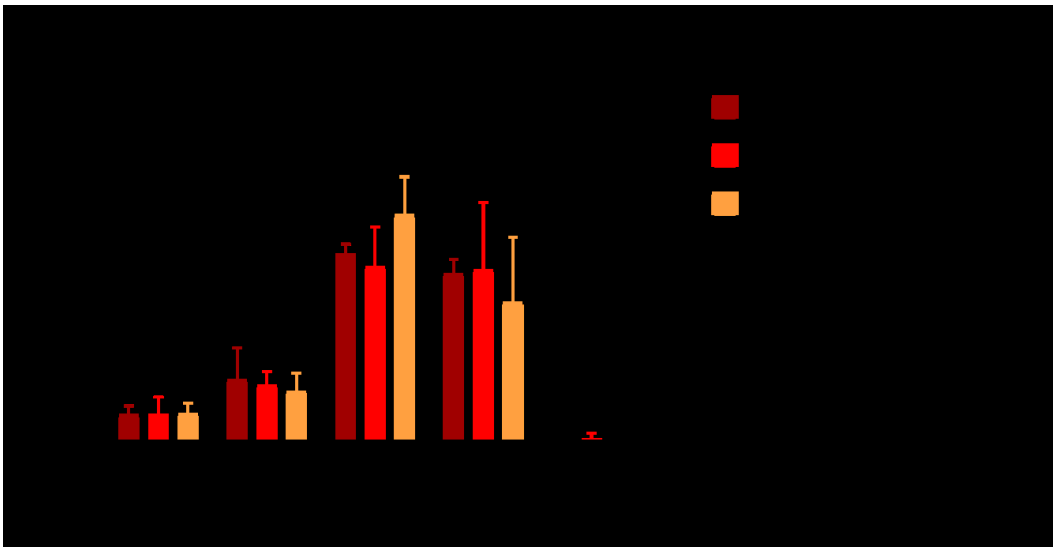

B

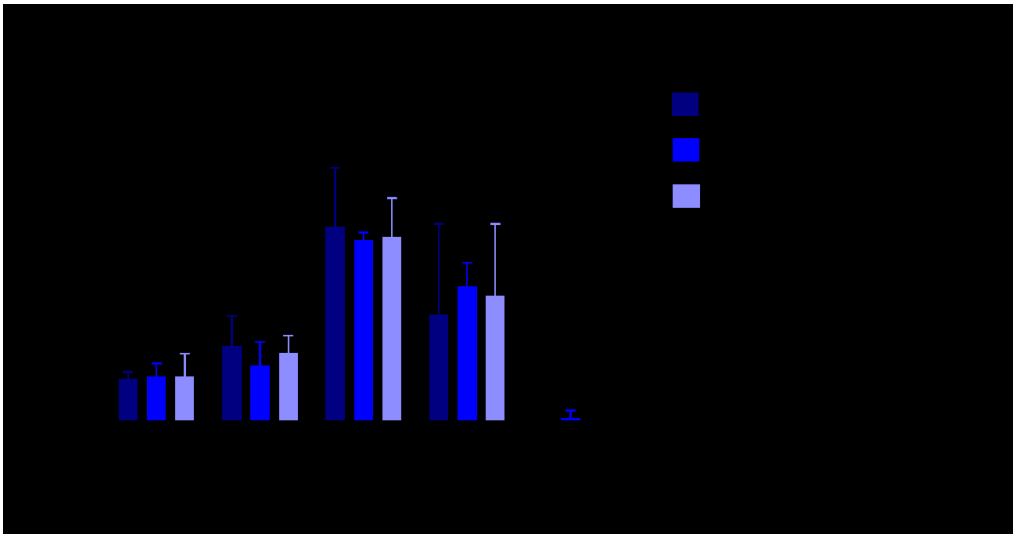

Figure 20-Intraceullar replication of *Δku80Δhxgprt*, *GRA3-mCherry* and *GRA7-mCherry* strains. Coverslips of HFF were infected with *Δku80Δhxgprt*, GRA3-mCherry or GRA7-mCherry expressing strains. The number of parasites per PV was counted after 20 hours of infection. The data shown are mean values ± SD from three independent experiments. No statistically significant differences between *Δku80Δhxgprt* and *GRA3-mCherry* or *GRA7-mCherry* strains were measured using a paired-T test. Figures were generated using Graph Pad Prism software.

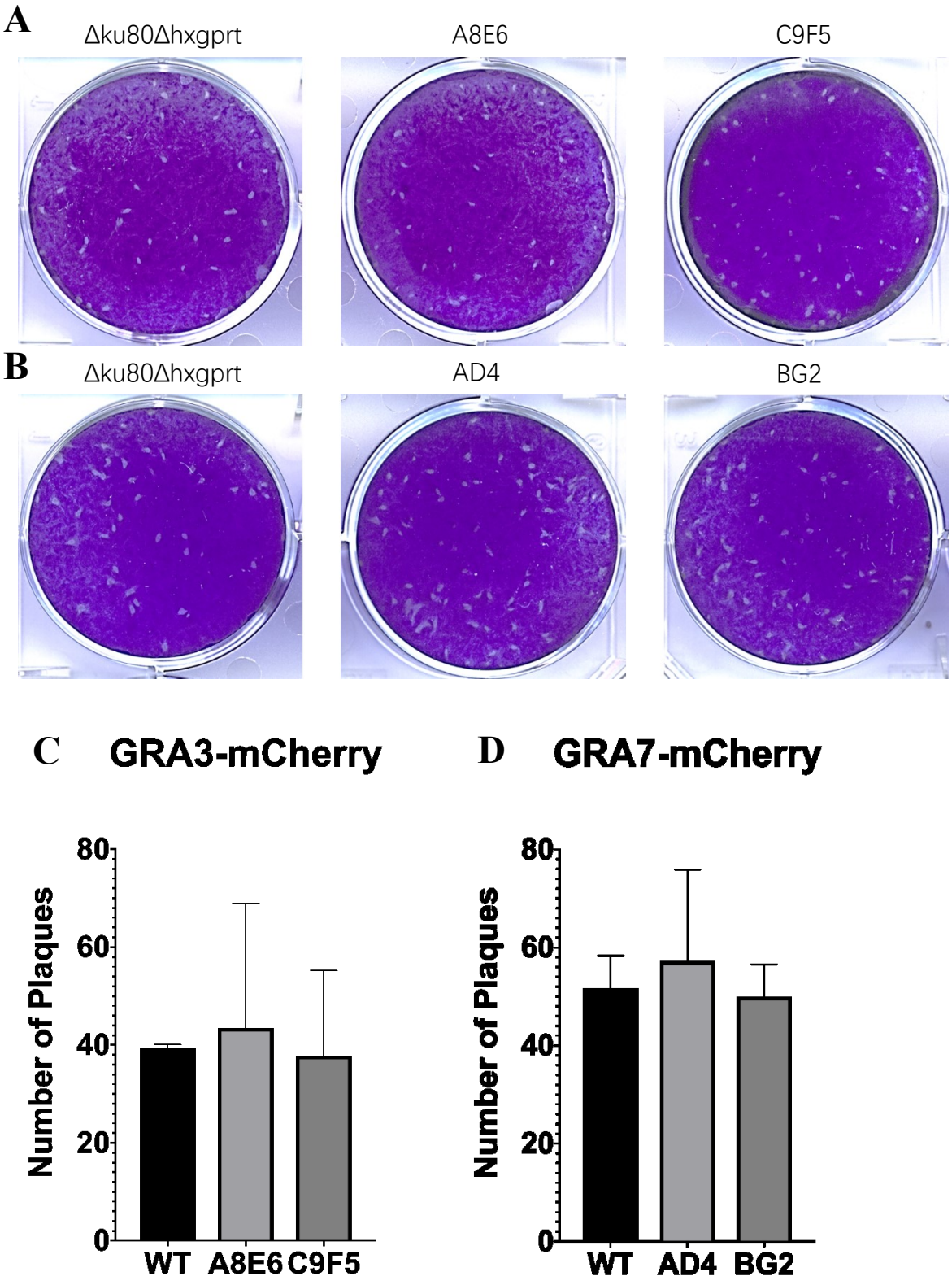
A
Δku80Δhxgprt
A8E6
C9F5
B
Δku80Δhxgprt
AD4
BG2
C
GRA3-mCherry
Number of Plaques
80
60
40
20
0
WT
A8E6
C9F5
D
GRA7-mCherry
Number of Plaques
80
60
40
20
0
WT
AD4
BG2

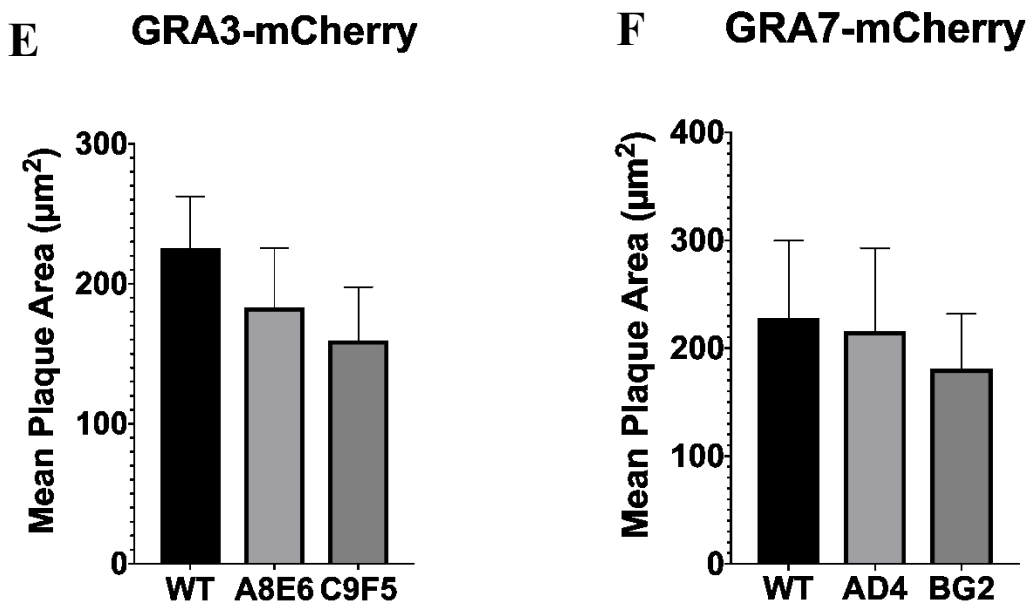

Figure 21-Plaque Assays of *Δku80Δhxgprt*, *GRA3-mCherry* and *GRA7-mCherry* strains. HFF were infected with 100 parasites of each strain and incubated at 37°C for 6 days. Two clonal populations of *GRA3-mCherry* or *GRA7-mCherry* were used. After incubation, cells were fixed with 100% ethanol and stained with crystal violet. The number of plaques was counted, and the area of each plaque was measured using Volocity software. The data shown are mean values ± SD from three independent experiments. No statistically significant difference was measured using a one-way ANOVA test. Figures were generated using Graph Pad Prism software. WT: *Δku80Δhxgprt* strain. AD4 and BG2: 2 clonal populations of *GRA7-mCherry* strain. A8E6 and C9F5: 2 clonal populations of *GRA3-mCherry* strain.

F. Live cell imaging

We chose the GRA3-mCherry expressing strains for live cell imaging because these strains have a better GRA3-mCherry signals and the mCherry is not cleaved in the parasite. We infected HFF cells with GRA3-mCherry expressing parasites and monitored events at the PV dynamically through time-lapse analysis. The PVM, dense granules and IVN were labeled by GRA3-mCherry, which is shown in white (Figure 22). Dense granule organelles were observed moving around inside the parasites (yellow box in Figure 22A). Two PV with close contact through their PVM were observed (Figure 22B). We observed that the IVN changed its shape during the movie (Figure 22B). For example, in the top PV, the IVN in the boxed region appeared to elongate; the IVN appeared to contact in the lower PV in the boxed region. PVM projections (PVMP) were observed connecting two PV (Figure 22C) and were observed extending into the host cytoplasm (Figure 22D, 22E, and 22F). PVMP was found to connect two PVs (Figure 22D) though little to no movement was detected in the time frame observed. Multiple PVMP of different lengths were detected extending from one PV. Potential movements of the longer PVMP, which is greater than 10 μm, was indicated with red arrows in Figure 22 D. The shorter PVMP, which was shorter than 5 μm, (yellow box in Figure 22E and 22F) retracted and elongated during the different time points, showing that the PVMP can be dynamic.

To study interactions between host vesicles and the PVM, we infected VERO cells stably expressing GFP-tagged Rab11A with GRA3-mCherry expressing parasites. In time-lapse microscopy, host GFP-Rab11A vesicles were observed inside the PV or close to the PVM (Figure 23). GFP-Rab11A vesicles found inside the PV localized primarily to the IVN region and most remained in the same area with little movement during the time frame

of the movie (Figure 23 B and 23C; white box). Some vesicles, however, were detected to move along the IVN (Figure 23 A and D; white box). These findings may indicate possible interactions between the IVN and host GFP-Rab11A vesicles inside PV. Some GFP-Rab11A vesicles moved to the PV and closely contacted the PVM. In some cases, the host vesicle remained in contact with the PVM throughout the duration of the movie (Figure 23D; blue arrows) or transiently contacted the PVM (Figure 23B, and 23D; white arrows). In Figure 24E, a GFP-Rab11A vesicle was first found to contact the PVM and then was found inside the PV 20 sec later, indicating the possible entry of host GFP-Rab11A vesicles through the PVM.

A

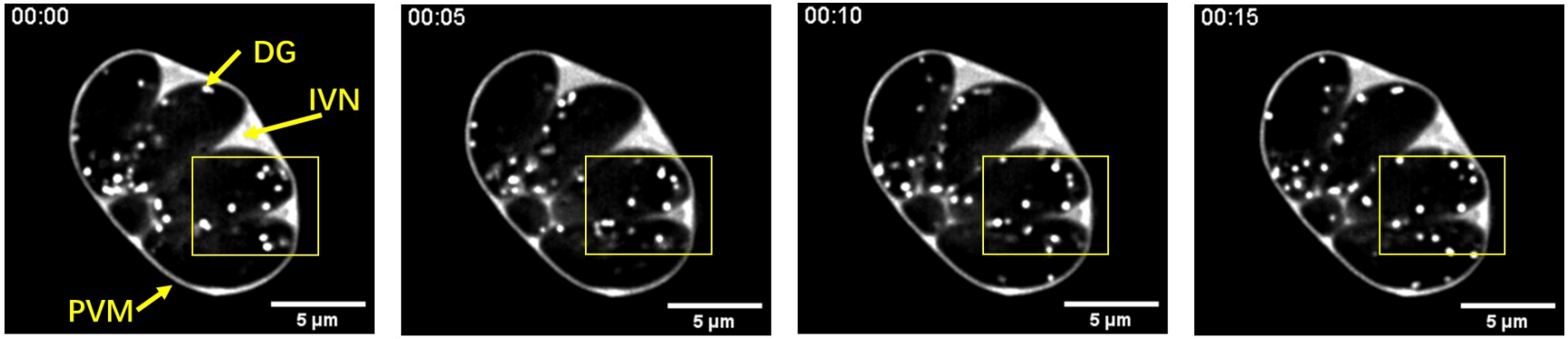
00:00
DG
IVN
PVM
5 µm
00:05
5 µm
00:10
5 µm
00:15
5 µm

B

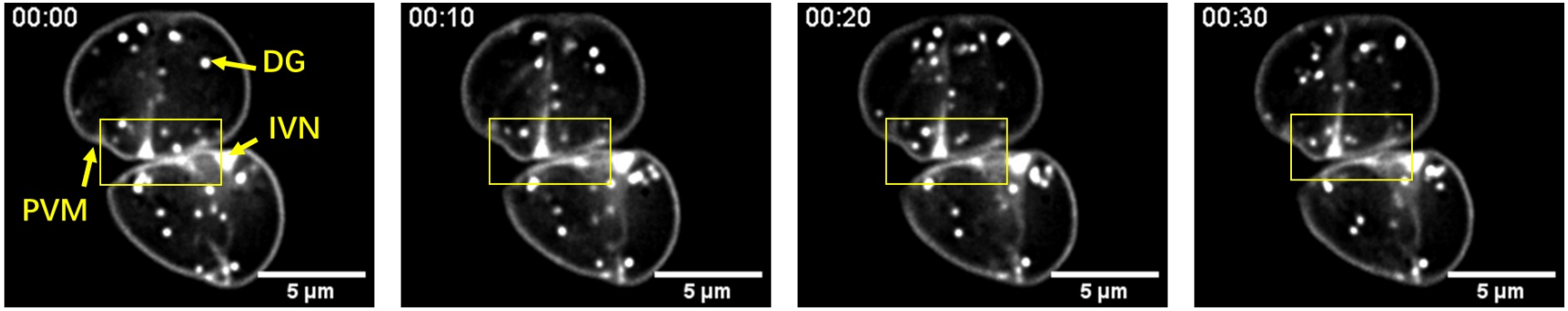
00:00
DG
IVN
PVM
5 µm
00:10
5 µm
00:20
5 µm
00:30
5 µm

C

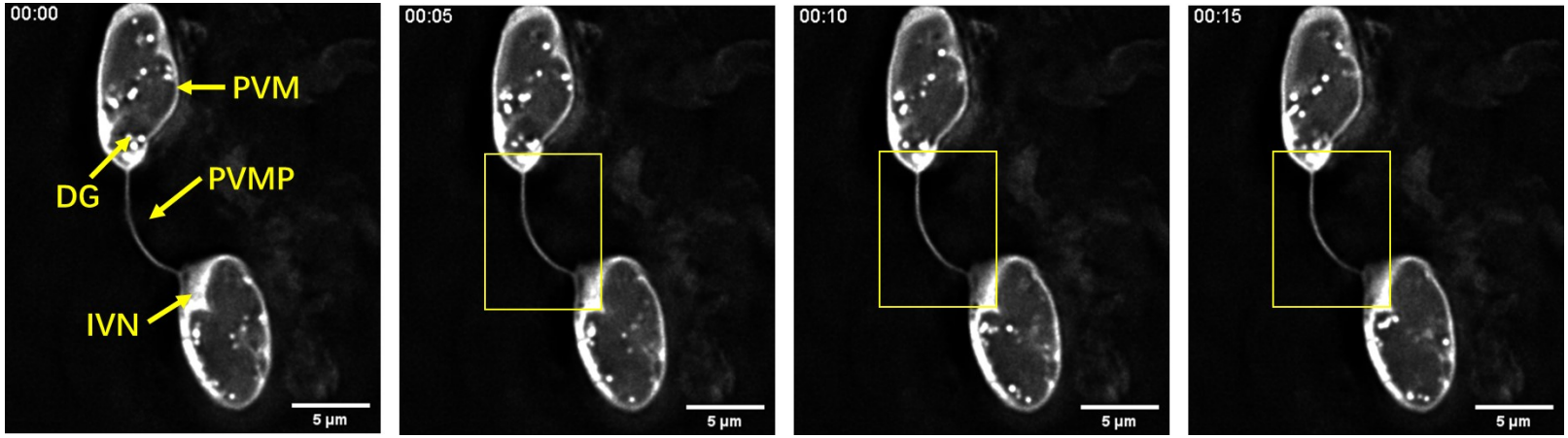
00:00
PVM
DG
PVMP
IVN
5 µm
00:05
5 µm
00:10
5 µm
00:15
5 µm

D

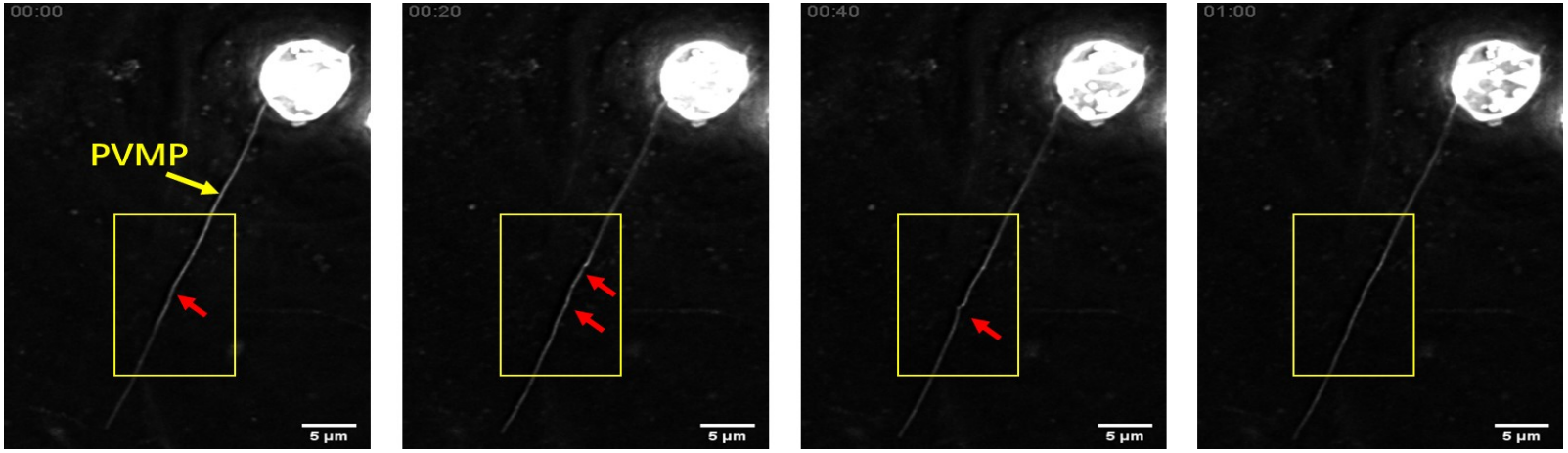
00:00
PVMP
5 µm
00:20
5 µm
00:40
5 µm
01:00
5 µm

E

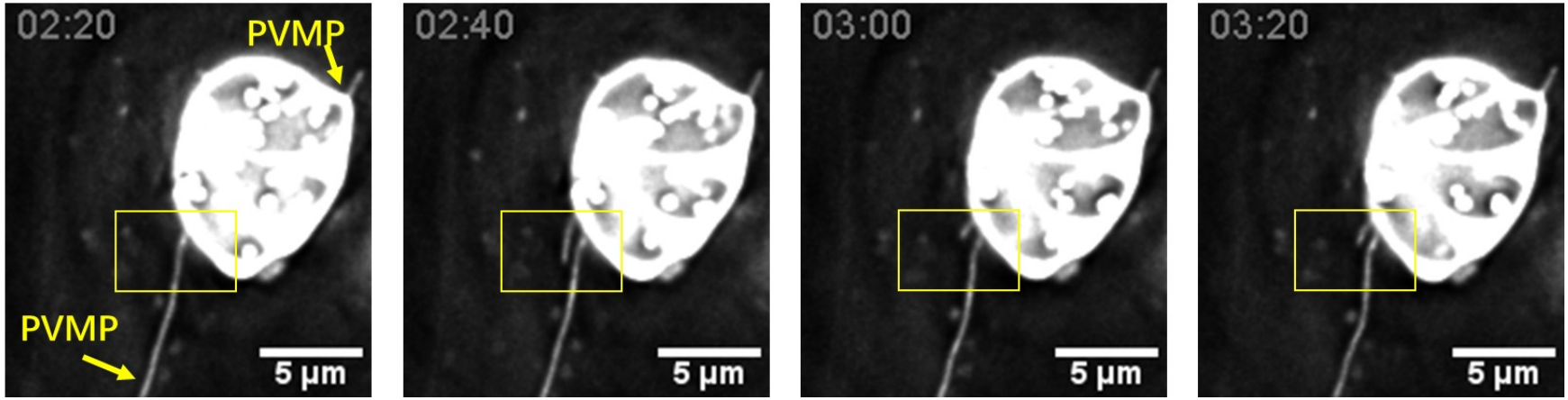
02:20
PVMP
PVMP
5 µm
02:40
5 µm
03:00
5 µm
03:20
5 µm

F

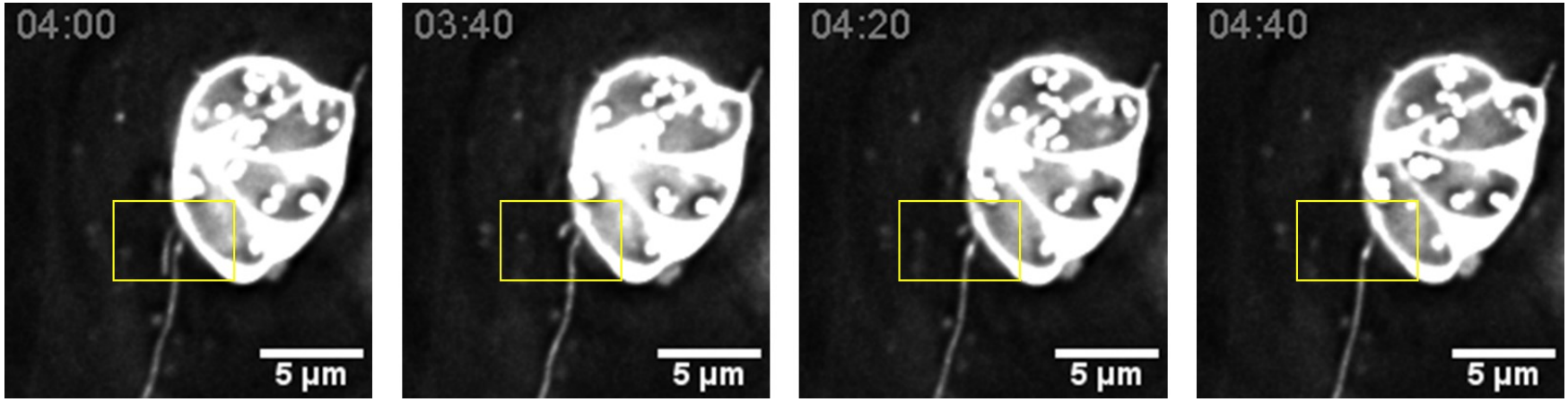
04:00
5 µm
03:40
5 µm
04:20
5 µm
04:40
5 µm

Figure 22-Snapshots of the PV of GRA3-mCherry expressing parasites at different time points. HFF cells were infected with GRA3-mCherry expressing parasites for 20 hours. Live cell imaging was done using the Delta Vision Elite Deconvolution Microscope. Images were processed and adjusted using ImageJ. Time (left top) and scale bars (right bottom) are shown. GRA3-mCherry is detected on the PVM, dense granules and IVN. Movement of dense granules and IVN can be observed at different time points. A) a single 4-parasite PV with movements of dense granules in the yellow square; Duration=2 min, Time lapse=5 sec. B) close contact between 2 PVs through PVM highlighted in the yellow square; Duration=2 min, Time lapse=5 sec. C) 2 PVs connected with each other through a PVMP in a yellow square; Duration=30 sec, Time lapse=5 sec. D, E & F) a single 4-parasite PV with extensions and retraction of a PVMP; Duration=5 min, Time lapse=20 sec. Potential movements of the PVMP in D was indicated with red arrows in yellow box. Movements of PVMP in E & F was highlighted in yellow box Brightness and contrast settings were increased to show PVMP in C, D, E, &F. IVN=tubulovesicular network of membranous tubules; PVM=parasitophorous vacuole membrane; DG=dense granule. PVMP=PVM projection.

A

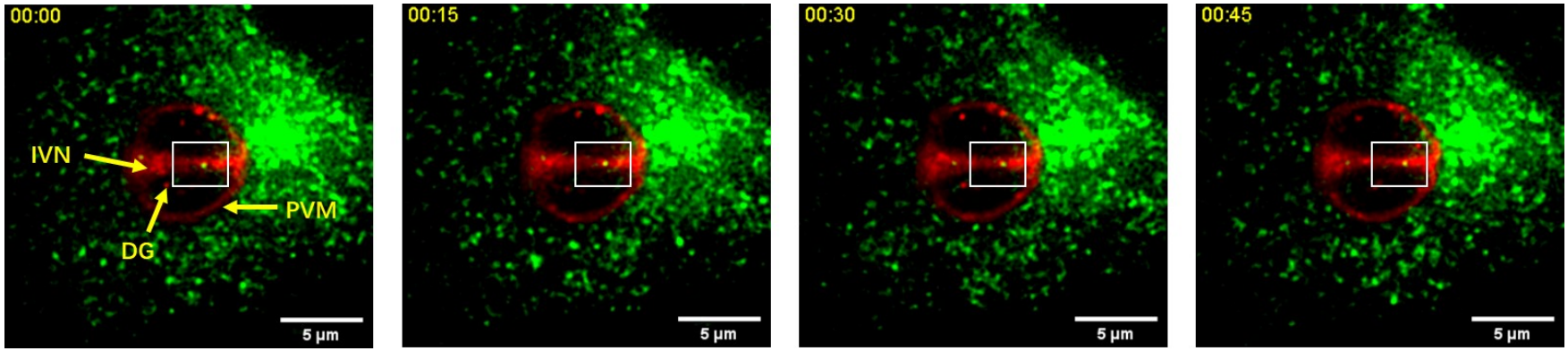
00:00
IVN
PVM
DG
5 µm
00:15
5 µm
00:30
5 µm
00:45
5 µm

B

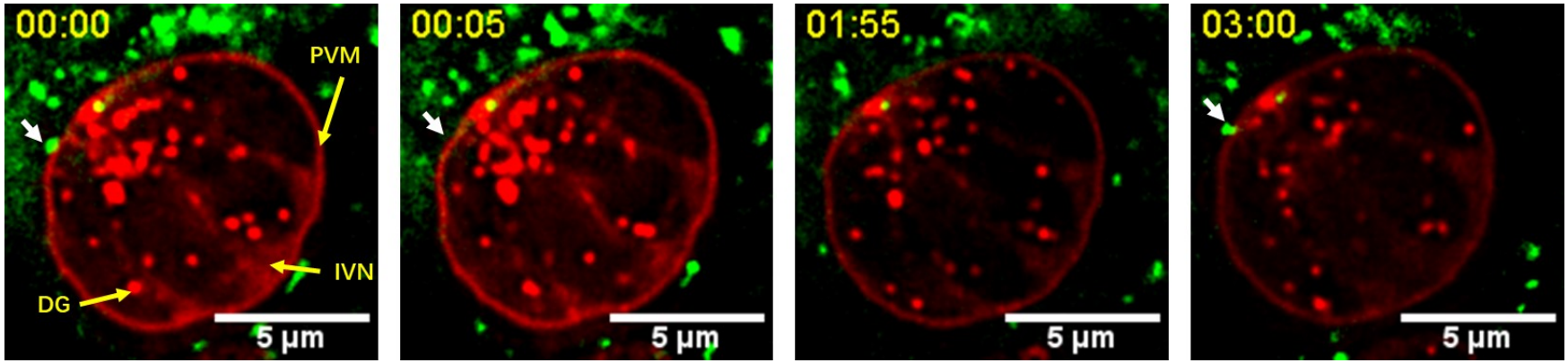
00:00
PVM
IVN
DG
5 µm
00:05
5 µm
01:55
5 µm
03:00
5 µm

C

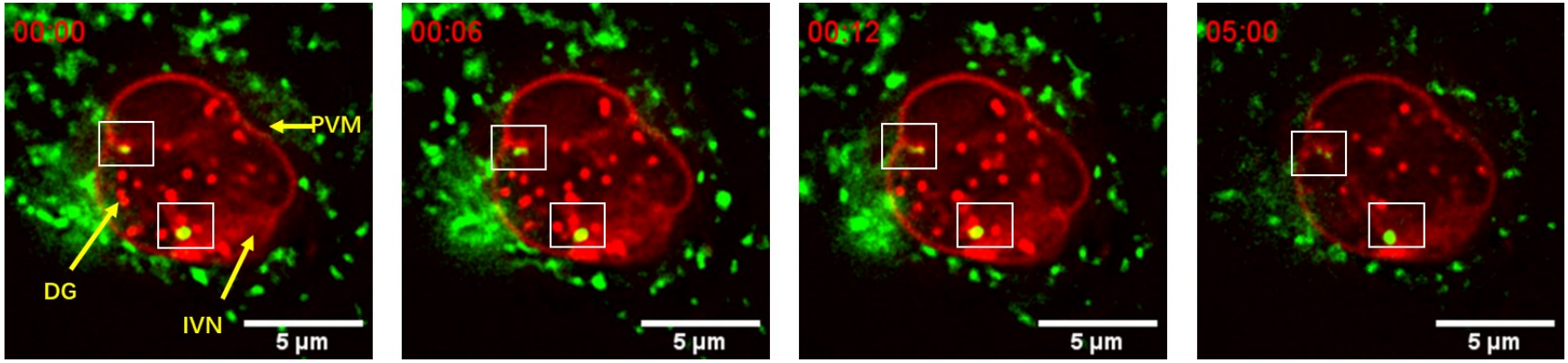
00:00
PVM
DG
IVN
5 µm
00:06
5 µm
00:12
5 µm
05:00
5 µm

D

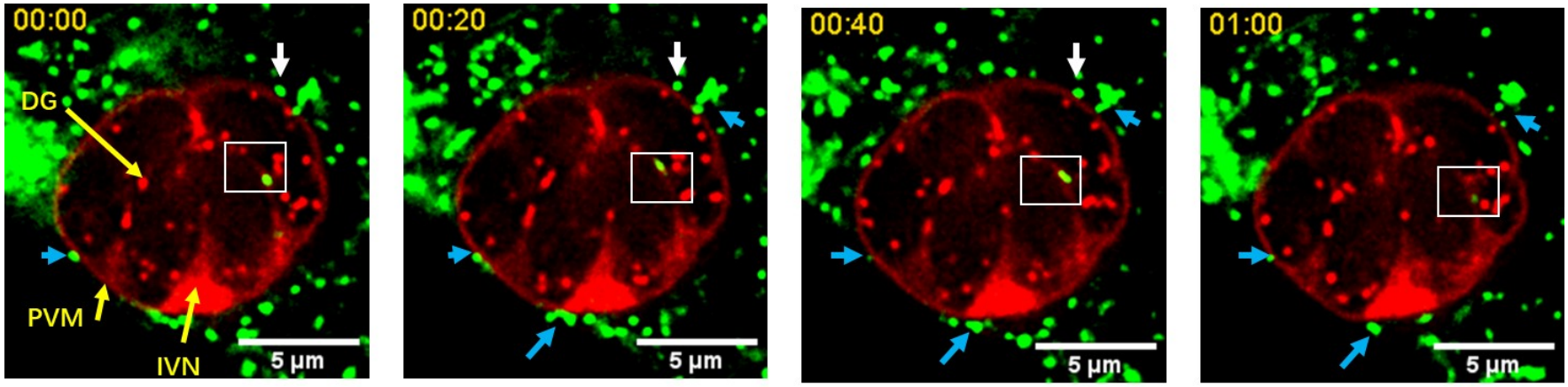
00:00
DG
PVM
IVN
5 µm
00:20
5 µm
00:40
5 µm
01:00
5 µm

E

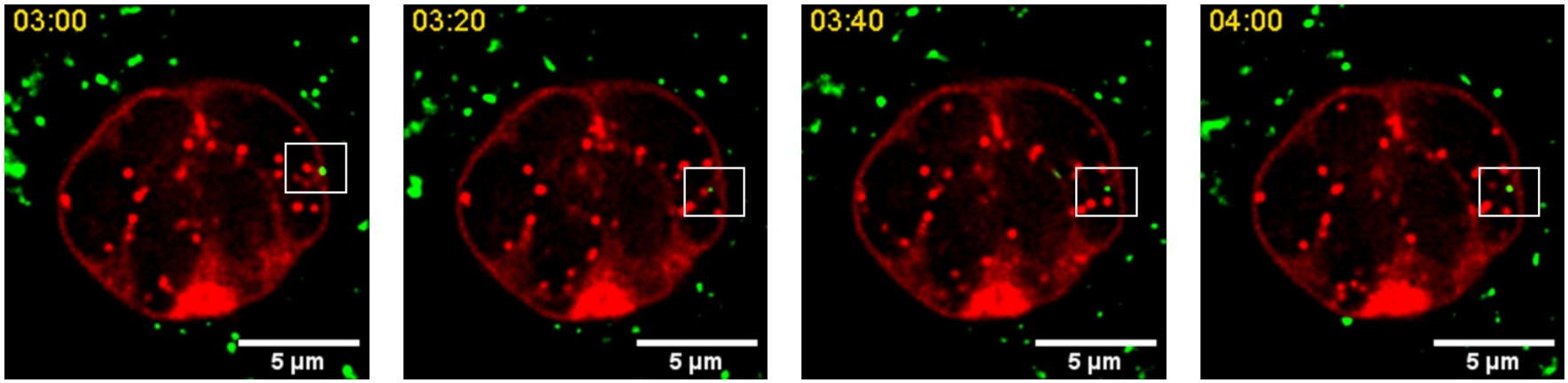

Figure 23-Interactions between host Rab11A vesicles and the PVM. VERO cells stably expressing GFP-Rab11 (green) were infected with GRA3-mCherry expressing parasites for 20 hours. Live cell imaging was done using a Delta Vision Elite Deconvolution Microscope. Images were processed and adjusted using ImageJ. PVM, dense granules and IVN are labeled by GRA3-mCherry, shown in red. Time (left top) and scale bars (right bottom) are shown. Host GFP-Rab11A vesicles found in the PV are highlighted with white squares. Host GFP-Rab11 vesicles found to stay close to the PVM for the entire video are indicated with blue arrows. Host GFP-Rab11 vesicles found to close contact to the PVM and then left are indicated with white arrows. Images from D & E are the same PV but different z-slices. The fourth image in panel C, and images in panel E were adjusted due to photobleaching. IVN=tubulovesicular network of membranous tubules; PVM=parasitophorous vacuole membrane; DG=dense granule. A) Duration=5 min, Time lapse=15 sec. B) Duration=5 min, Time lapse=5 sec. C) Duration=5 min, Time lapse=5 sec. D & E) Duration =10 min, Time lapse=20 sec.

4. DISCUSSION:

Toxoplasma is an obligate intracellular parasite that scavenges host nutrients for survival. Previous data from our lab has shown that *T. gondii* intercepts host Rab trafficking pathways and internalizes host Rab vesicles into the PV (Romano et al., 2017a; Romano et al., 2013), possibly for nutrient acquisition. As the PVM does not fuse with these host vesicles, the mechanisms of Rab vesicles internalization into the PV is not clear. To further explore the mechanism, requires a dynamic view of the interactions between host vesicles and the PVM. Therefore, the major goal of my master's thesis is to generate parasite strains expressing fluorescent markers on the PVM and analyze the movement of the PVM over time relative to host Rab vesicles through live cell imaging.

To study the dynamic interactions between the PVM and host organelles, we successfully engineered *Toxoplasma* strains that stably express a fluorescently-labeled PVM protein, either GRA3 or GRA7, using the CRISPR/Cas9 system. This gene editing system was able to specifically target GRA3 or GRA7 for the insertion of mCherry at the 3' end of the gene with high efficiency. We confirm that the insertion of mCherry does not affect parasite replication based on microscopy growth assays nor does it affect invasion, replication or egress based on plaque assays. The mCherry-labeled GRA3 protein localized to the dense granules, IVN and PVM, which has a similar localization pattern compared to antibody localized GRA3 in the parental strain. However, most GRA7-mCherry protein localizes to the dense granules rather than the PVM or IVN. In addition, a higher colocalization level was measured for *GRA3-mCherry* strain than for *GRA7-mCherry* strain when comparing the signals of mCherry and antibody localized GRA3 or GRA7. It is possible that the difference in colocalization between mCherry and anti-GRA7 antibody

fluorescence is due to cleavage of mCherry from the GRA7 protein in the dense granules, which correlates with the results of the western blot analysis. Another possibility would be that mCherry masks some GRA7 antigens. As a result, the GRA3-mCherry expressing strains were selected for live cell imaging.

GRA3-mCherry expressing parasites show us a clearly dynamic view of the PVM, IVN and dense granules. Through live cell imaging, we observed rapid movement of dense granules inside parasites and the IVN in the PV. We also observed contacts between two PVs either through a direct PVM-PVM or PVMP connection, indicating that the PVM might play a role in the interaction between two PVs. PVMP, which is decorated with GRA proteins (Dubremetz et al., 1993; Jacobs et al., 1998; Rome et al., 2008; Romano et al., 2013), is a unique feature of the PVM. Several previous studies have shown that PVMP extend throughout the host cytosol and can interact with host organelles. For example, PVMP are found to contact the microtubule-organizing center (MTOC), Golgi, or other PVs in the same host cell or adjacent cells (Coppens et al., 2006; Rome et al., 2008), indicating its dynamic nature. In this study, we were the first to observe the dynamics of PVMPs in live cells. We observed one PV with three PVMPs extending into host cytosol– two short PVMPs (less than 5μm) and one more than 10μm. One of the short PVMPs retracted and elongated into the host cytosol during a 140-sec time frame, while no movement was observed for the other short one. Partial movements were observed for the long PVMP. No movement was observed for the PVMP connecting between two PV as well. Our observations indicate that PVMP can be very diverse, either being dynamic or motionless. To gain the number of PVMP forms per PV, and how stable they are, it would

be interesting to investigate PVMP dynamics during a longer time period by live cell imaging.

Previous studies have shown that host Rab vesicles involved in anterograde, recycling, and endocytic pathways, are found inside the PV (Nolan et al., 2017; Romano et al., 2017; Romano et al., 2013). To investigate the interactions between host vesicles and the PVM, we infected VERO cells stably expressing GFP-Rab11a with GRA3-mCherry expressing parasites. Previous studies in our lab have shown that the IVN contributes to host vesicle sequestration (Romano et al. 2017), and we were able to confirm this role for IVN in our study. Host GFP-Rab11A vesicles were localized in the IVN region and some of them appeared to be transported along the IVN at different time points. This observation might indicate that the IVN not only plays a role in sequestering host vesicles, but may also play a role in transporting host vesicles inside the PV.

Interactions between the PVM and host Rab11A vesicles are diverse. We observed that some host Rab11A vesicles remain closely associated with the PVM while others only briefly contact the PVM. In one PV, a host Rab11A vesicle was first observed to closely contact the PVM, and then was found inside the PV, in the IVN region. This finding, along with evidence from previous studies (Romano et al., 2017a; Romano et al., 2013), suggests that host Rab vesicles can cross the PVM to be fully internalized into the PV. However, we were not able to capture the moment of host vesicle entry into the PV, because the exposure time for GFP-Rab11A was too long to allow for a short enough time-lapse setting. To overcome this problem, we are now creating a cell line that stably expresses mEmerald-Rab11A, which should be brighter and more photostable, thus allowing for a shorter exposure settings and consequently smaller intervals between time-lapse timepoints.

Two different mechanisms have been described for the entry of host vesicles into the PV. In one, the entry of host vesicles may be facilitated by host microtubules pushing into the PVM, forming invaginations that function as conduits, which are termed "host organelle-sequestering tubule structures" or H.O.S.T. (Coppens et al. 2006; Romano et al., 2013). In the other, host Rab vesicles may be internalized into regions where the tubules of the IVN connect to and fuse with the PVM, forming conduits or gate of entry for host vesicles (Romano et al., 2017). It would be interesting to use live cell imaging to inspect the dynamic of host microtubules pocking onto the PVM at location where host vesicles penetrate the PV.

FUTURE DIRECTIONS:

In summary, we successfully created a *Toxoplasma* strain that stably expresses a fluorescently labeled PVM protein. Using this strain, we were able to study the dynamic movements of PVMP, and interactions between the PVM and host Rab vesicles through live cell imaging. For future studies, we are interested in investigating how host Rab11A vesicles pass through the PVM into the PV. We are also interested in studying the function of PVMPs, as well as their interactions with host organelles.

Toxoplasma PVM not only interacts with host Rab vesicles, but also with other host organelles. After invasion, multiple host organelles are recruited to and associate with the PV, a process that is hypothesized to function in nutrient acquisition by the parasite. (Coppens, 2014). For example, parasite growth is dependent on lipoate from host mitochondria, thus, making PV-associated mitochondria a possible source for this metabolite (Crawford et al. 2006). Other studies provide evidence that *T. gondii* may scavenge phospholipids from the ER (Pratt et al., 2013), indicating a role for PVM-

associated ER in lipid acquisition. The host Golgi, which associates with the PV, is also a source of sphingolipids for the parasite (Romano et al., 2013). In addition, association between the PV and MTOC results in the reorganization of the microtubular network around the PV and recruitment of host vesicles to the PV (de Melo and De Souza, 1996; Coppens et al., 2006; Romano et al., 2013). However, the molecular mechanisms of these interactions between the PVM and host organelles, for nutrition acquisition, remain to be determined. Besides, these previous findings are all based on fixed cells analyzed by fluorescence and electron microscopy. Therefore, we are interested in studying the dynamic interactions between PVM and other host organelles in more details over time. By infecting cells expressing different organelle markers with the GRA3-mCherry expressing parasites, we will be able to investigate PVM-host organelle interactions through live cell imaging at different points during infection. Also, adding fluorescently labeled lipids to the medium of cells infected with GRA3-mCherry expressing parasites, we will be able to analyze the role of the PVM and IVN in the internalization of host lipids into the PV.

A better understanding of how the PVM interacts with host organelles, the parasite internalizes host vesicles into its PV and scavenges host lipids from intra-PV vesicles will provide insight important for our long-term goal of identifying possible drug targets to treat *Toxoplasma* infections in the nutrient salvage pathways These potential drug targets can be parasite effectors that attach to host organelles or vesicles, internalize host vesicles or release host nutrients from host organelles or vesicles. Molecular interference with these effectors may deplete nutrients or disrupt scavenging activities, which starves and kills *T. gondii*.

REFERENCE:

1. Zhao, T., et al., Immunogenicity of induced pluripotent stem cells Immunogenicity of induced pluripotent stem cells. Nature, 2011. 474 (7350): p. 212-215.
2. Zhang, F., X. Guo, and Y. Wen, CRISPR/Cas9 for genome editing: progress, implications and challenges. Human Molecular Genetics, 2014. 23(R1): p. R40-R46.
3. Wang, Z.-D., et al., Prevalence and burden of *Toxoplasma gondii* infection in HIV-infected people: a systematic review and meta-analysis. The Lancet HIV, 2017. 4(4): p. 177-188.
4. Wang, J.L., et al., Evaluation of the basic functions of six calcium-dependent protein kinases in Toxoplasma gondii using CRISPR-Cas9 system. Parasitology Research, 2016. 115(2): p. 697-702.
5. Walker, M.E., et al., *Toxoplasma gondii* actively remodels the microtubule network in host cells. Microbes and Infection, 2008. 10 (14-15): p. 1440-1449.
6. Vinayak, S., et al., Genetic Manipulation of the *Toxoplasma gondii* genome by fosmid recombineering. mBio, 2014. 5(6): p. e02021-14.
7. Torgerson, P.R. and P. Mastroiacovo, The global burden of congenital toxoplasmosis: a systematic review. Bull World Health Organ, 2013. 91(7): p. 501-508.
8. Tonkin, M.L., et al., Host Cell Invasion by Apicomplexan Parasites: Insights from the Co-Structure of AMA1 with a RON2 Peptide. Science, 2011. 333(6041): p. 463-467.
9. Sinai, A.P., P. Webster, and K.A. Joiner, Association of host cell endoplasmic reticulum and mitochondria with the *Toxoplasma gondii* parasitophorous vacuole membrane: a high affinity interaction. The Journal of Cell Science, 1997. 110 (Pt 17): p. 2117-2128.
10. Sibley, L.D., et al., Regulated secretion of multi-lamellar vesicles leads to formation of a tubulo-vesicular network in host-cell vacuoles occupied by *Toxoplasma gondii*. The Journal of Cell Science, 1995. 108 (Pt 4): p. 1669-1677.
11. Shen, B., et al., Efficient Gene Disruption in Diverse Strains of *Toxoplasma gondii* using CRISPR/CAS9. mBio, 2014. 5(3): p. e01114-14.
12. Shen, B., et al., Development of CRISPR/Cas9 for efficient genome editing in *Toxoplasma gondii*. Methods in Molecular Biology, 2017. 1498: p. 79-103.
13. Seabra, S.H., et al., Endogenous polyamine levels in macrophages is sufficient to support growth of *Toxoplasma gondii*. The Journal of Parasitology, 2004. 90(3): p. 455-460.
14. Schwartzman, J.D. and E.R. Pfefferkorn, *Toxoplasma gondii*: Purine synthesis and salvage in mutant host cells and parasites. Experimental Parasitology, 1982. 53(1): p. 77-86.
15. Schwab, J.C., C.J. Beckers, and K.A. Joiner, The parasitophorous vacuole membrane surrounding intracellular Toxoplasma gondii functions as a molecular sieve. Proceedings of the National Academy of Sciences of the United States of America, 1994. 91(2): p. 509-513.
16. Schindelin, J., et al., Fiji: an open-source platform for biological-image analysis. Nature Methods, 2012. 9(7): p. 676-682.

17. Rosowski, E.E., et al., Strain-specific activation of the NF-κB pathway by GRA15, a novel *Toxoplasma gondi* dense granule protein. The Journal of Experimental Medicine, 2011. 208(1): p. 195-212.
18. Rome, M.E., et al., Intervacuolar Transport and Unique Topology of GRA14, a Novel Dense Granule Protein in *Toxoplasma gondii*. Infection and Immunity, 2008. 76(11): p. 4865-4875.
19. Romano, J.D., et al., *Toxoplasma gondii* salvages sphingolipids from the host Golgi through the rerouting of selected Rab vesicles to the parasitophorous vacuole. Molecular Biology of the Cell, 2013. 24(12): p. 1974-1995.
20. Romano, J.D., et al., The parasite *Toxoplasma* sequesters diverse Rab host vesicles within an intravacuolar network. The Journal of Cell Biology, 2017. 216(12): p. 4235-4254.
21. Robert-Gangneux, F. and M.-L. Dardé, Epidemiology of and diagnostic strategies for Toxoplasmosis. Clinical Microbiology Reviews, 2012. 25(2): p. 264-296.
22. Rajapakse, S., et al., Antibiotics for human Toxoplasmosis: a systematic review of randomized trials. Pathogens and Global Health, 2013. 107(4): p. 162-169.
23. Pratt, S., et al., Sphingolipid synthesis and scavenging in the intracellular apicomplexan parasite, *Toxoplasma gondii*. Molecular and Biochemical Parasitology, 2013. 187(1): p. 43-51.
24. Pfefferkorn, E.R., Interferon gamma blocks the growth of *Toxoplasma gondii* in human fibroblasts by inducing the host cells to degrade tryptophan. Proceedings of the National Academy of Sciences of the United States of America, 1984. 81(3): p. 908-912.
25. Nolan, S.J., J.D. Romano, and I. Coppens, Host lipid droplets: An important source of lipids salvaged by the intracellular parasite *Toxoplasma gondii*. Public Library of Science Pathogens, 2017. 13(6): p. e1006362.
26. Neville, A.J., et al., Clinically available medicines demonstrating anti-*Toxoplasma* activity. Antimicrobial Agents and Chemotherapy, 2015. 59(12): p. 7161-7169.
27. Nam, H.W., GRA proteins of *Toxoplasma gondii*: maintenance of host-parasite interactions across the parasitophorous vacuolar membrane. The Korean Journal of Parasitology, 2009. 47 Suppl: p. S29-37.
28. Moudy, R., T.J. Manning, and C.J. Beckers, The loss of cytoplasmic potassium upon host cell breakdown triggers egress of *Toxoplasma gondii*. The Journal of Biological Chemistry, 2001. 276(44): p. 41492-41501.
29. Mordue, D.G., et al., Invasion by *Toxoplasma gondii* establishes a moving junction that selectively excludes host cell plasma membrane proteins on the basis of their membrane anchoring. The Journal of Experimental Medicine, 1999. 190(12): p. 1783-1792.
30. Montazeri, M., et al., A systematic review of in vitro and in vivo activities of anti-*Toxoplasma* drugs and compounds (2006-2016). Frontiers in Microbiology, 2017. 8: p. 25-25.
31. Molestina, R.E., et al., Activation of NF-κB by *Toxoplasma gondii* correlates with increased expression of antiapoptotic genes and localization of phosphorylated IκB to the parasitophorous vacuole membrane. The Journal of Cell Science, 2003. 116(21): p. 4359-4371.

32. Miller, C.M., et al., The immunobiology of the innate response to *Toxoplasma gondii*. The International Journal for Parasitology, 2009. 39(1): p. 23-39.
33. Mercier, C., et al., Biogenesis of nanotubular network in *Toxoplasma* parasitophorous vacuole induced by parasite proteins. Molecular Biology of the Cell, 2002. 13(7): p. 2397-2409.
34. Mercier, C. and M.-F. Cesbron-Delauw, *Toxoplasma* secretory granules: one population or more? Trends in Parasitology, 2015. 31(2): p. 60-71.
35. McCoy, J.M., et al., TgCDPK3 regulates calcium-dependent egress of *Toxoplasma* gondii from host cells. Public Library of Science Pathogens, 2012. 8(12): p. e1003066.
36. Martin, A.M., et al., The *Toxoplasma gondii* parasitophorous vacuole membrane: transactions across the border. The Journal of Eukaryotic Microbiology, 2007. 54(1): p. 25-28.
37. Ma, J.S., et al., Selective and strain-specific NFAT4 activation by the *Toxoplasma gondii* polymorphic dense granule protein GRA6. The Journal of Experimental Medicine, 2014. 211(10): p. 2013-2032.
38. Laliberté, J. and V.B. Carruthers, Host cell manipulation by the human pathogen Toxoplasma gondii. Cellular and Molecular Life Sciences, 2008. 65(12): p. 1900-1915.
39. Khan, A. and M.E. Grigg, *Toxoplasma gondii*: Laboratory maintenance and growth. Current Protocols in Microbiology, 2017. 44: p. 20c.1.1-20c.1.17.
40. Kafsack, B.F.C., et al., Rapid membrane disruption by a perforin-like protein facilitates parasite exit from host cells. Science, 2009. 323(5913): p. 530-533.
41. Jacobs, D., et al., Identification and heterologous expression of a new dense granule protein (GRA7) from *Toxoplasma gondii*. Molecular and Biochemical Parasitology, 1998. 91(2): p. 237-249.
42. Huynh, M.-H. and V.B. Carruthers, Tagging of endogenous genes in a *Toxoplasma gondii* strain lacking Ku80. Eukaryotic Cell, 2009. 8(4): p. 530-539.
43. Hussain, M.A., et al., *Toxoplasma gondii* in the food supply. Pathogens, 2017. 6(2): p. 21.
44. Goldszmid, R.S., et al., Host ER-parasitophorous vacuole interaction provides a route of entry for antigen cross-presentation in T*oxoplasma gondii*-infected dendritic cells. The Journal of Experimental Medicine, 2009. 206(2): p. 399-410.
45. Gold, D.A., et al., The *Toxoplasma* dense granule proteins GRA17 and GRA23 mediate the movement of small molecules between the host and the parasitophorous vacuole. Cell Host Microbe, 2015. 17(5): p. 642-652.
46. Gaji, R.Y., et al., Phosphorylation of a myosin motor by TgCDPK3 facilitates rapid initiation of motility during *Toxoplasma gondii* egress. Public Library of Science Pathogens, 2015. 11(11): p. e1005268.
47. Fox, B.A., J.P. Gigley, and D.J. Bzik, *Toxoplasma gondii* lacks the enzymes required for de novo arginine biosynthesis and arginine starvation triggers cyst formation. The International Journal of Parasitology, 2004. 34(3): p. 323-331.
48. Ferguson, D.J.P., Use of molecular and ultrastructural markers to evaluate stage conversion of *Toxoplasma gondii* in both the intermediate and definitive host. International The Journal for Parasitology, 2004. 34(3): p. 347-360.

49. Dubremetz, J.F., et al., Kinetics and pattern of organelle exocytosis during *Toxoplasma gondii*/host-cell interaction. Parasitology Research, 1993. 79(5): p. 402-408.
50. Dubey, J.P., et al., Sporulation and survival of *Toxoplasma gondii* oocysts in different types of commercial cat litter, 2011. Journal of Parasitology, 97(5): p.751-754
51. Dimier, I.H. and D.T. Bout, Interferon-gamma-activated primary enterocytes inhibit *Toxoplasma gondii* replication: a role for intracellular iron. Immunology, 1998. 94(4): p. 488-495.
52. de Melo, E.J. and W. de Souza, A cytochemistry study of the inner membrane complex of the pellicle of tachyzoites of Toxoplasma gondii. Parasitology Research, 1997. 83(3): p. 252-256.
53. de Melo, E.J., T.U. de Carvalho, and W. de Souza, Penetration of Toxoplasma gondii into host cells induces changes in the distribution of the mitochondria and the endoplasmic reticulum. Cell Structure and Function, 1992. 17(5): p. 311-317.
54. Cribbs, A. P., & Perera, S. (2017). Science and bioethics of CRISPR-Cas9 gene editing: an analysis towards separating facts and fiction. The Yale Journal of Biology and Medicine, 90(4), 625–634.
55. Crawford, M.J., et al., *Toxoplasma gondii* scavenges host-derived lipoic acid despite its de novo synthesis in the apicoplast. The European Molecular Biology Organization Journal, 2006. 25(13): p. 3214-3222.
56. Coster, L.O.B., Parasitic Infections in solid organ transplant recipients. Infectious Disease Clinics of North America, 2013. 27(2): p. 395-427.
57. Coppens, I., A.P. Sinai, and K.A. Joiner, *Toxoplasma gondii* exploits host low-density lipoprotein receptor-mediated endocytosis for cholesterol acquisition. The Journal of Cell Biololy, 2000. 149(1): p. 167-180.
58. Coppens, I. and K.A. Joiner, Host but not parasite cholesterol controls *Toxoplasma* cell entry by modulating organelle discharge. Molecular biology of the Cell, 2003. 14(9): p. 3804-3820.
59. Coppens, I., et al., *Toxoplasma gondii* Sequesters lysosomes from mammalian hosts in the vacuolar space. Cell, 2006. 125(2): p. 261-274.
60. Coppens, I., Exploitation of auxotrophies and metabolic defects in Toxoplasma as therapeutic approaches. The International Journal of Parasitology, 2014. 44(2): p. 109-120.
61. Charron, A.J. and L.D. Sibley, Host cells: mobilizable lipid resources for the intracellular parasite Toxoplasma gondii. The Journal of Cell Science, 2002. 115(15): p. 3049-3059.
62. Carruthers, V.B. and L.D. Sibley, Sequential protein secretion from three distinct organelles of *Toxoplasma gondii* accompanies invasion of human fibroblasts. The European Journal of Cell Biololy, 1997. 73(2): p. 114-123.
63. Boyer, K., et al., Unrecognized ingestion of *Toxoplasma gondii* oocysts leads to congenital Toxoplasmosis and causes epidemics in North America. Clinical Infectious Disease, 2011. 53(11): p. 1081-1089.
64. Blader, I.J., et al., Lytic cycle of *Toxoplasma gondii*: 15 years later. Annual Review of Microbiology, 2015. 69: p. 463-485.

65. Beghetto, E., et al., Identification of a human immunodominant B-cell epitope within the GRA1 antigen of *Toxoplasma gondii* by phage display of cDNA libraries. The International Journal of Parasitology, 2001. 31(14): p. 1659-1668.
66. Barrangou, R., et al., CRISPR provides acquired resistance against viruses in prokaryotes. Science, 2007. 315(5819): p. 1709-1712.
67. Bai, M. J., et al., Functional characterization of dense granule proteins in *Toxoplasma gondii* RH strain using CRISPR-Cas9 system. Frontiers in Cellular and Infection Microbiology, 2018. 8(300).

LUQIONG WANG

108W.39th Street, Baltimore, MD, 21210
Mobile phone:920-931-5682; luqiong.wang113@gmail.com

EDUCATION:

Johns Hopkins Bloomberg School of Public Health, Baltimore, MD May 2019

- Master of Science in Molecular Microbiology and Immunology

Lawrence University, Appleton, WI Aug 2013-Jun 2017

- Bachelor of Arts in Biology & minor in Anthropology

RESEARCH EXPERIENCES:

- ***Master Thesis & Research Assistant***, Coppens Lab

Johns Hopkins School of Public Health, Baltimore, MD Nov 2017-Present

Title: Investigating the Dynamics of the Interaction between Mammalian Host Organelles and *Toxoplasma*

The goal of my thesis research is to investigate the dynamic interaction between mammalian host organelles, such as GFP-Rab-11 vesicles, and the parasitophorous vacuole membrane (PVM) of *Toxoplasma* through live cell imaging. To achieve this goal, I engineered *Toxoplasma* strains that stably express a fluorescently-labeled (mCherry) PVM protein (GRA3 or GRA7) using CRISPR/Cas9. I designed primers and performed PCR to confirm the insertion of *mCherry* in the correct location in the parasite genome. I also performed growth and localization assays to confirm that tagging GRA3 and GRA7 does not alter the localization of the proteins or the ability of the parasites to grow normally. Following confirmation, I used these strains for live cell imaging to observe the interaction between host GFP-Rab-11 vesicles and the PVM. Those parasite strains will also be valuable as a tool to study various interactions between PVM and other host organelles in future research.

- ***Senior Capstone Project***, Humphries Lab

Lawrence University, Appleton, WI Sept 2016-Jun 2017

Title: Molecular characterization and immune responses of macrophage expressed gene from freshwater snail, *Biomphalaria glabrata*

Macrophage expressed genes (Mpegs) encode members of the membrane-attack complex/perforin protein superfamily that have been shown to play essential roles in antibacterial activities in some mollusks. The role of Mpegs is unknown in the freshwater snail, *Biomphalaria glabrata*, which is the vector of *Schistosoma mansoni*. To understand its role in *B.glabrata*, I first used different genetic analysis tools to characterize Mpeg in the snail genome, determined their distribution in various snail tissues, and compared its homologs to those of other species. I then designed and optimized protocols for cloning, expressing and purifying one of the *B.glabrata* Mpeg proteins I identified in bacteria for future immunological assays. By the end of my project, I was able to detect purified Mpeg protein with an anti-human Mpeg antibody, which proves its conservation across species.

- ***Summer Research Assistant,*** LaBelle Lab

University of Chicago, Chicago, IL Jun 2016-Aug 2016

Title: Cloning of CD19 single chain variable fragment (scFv) for a new peptide-based therapeutic delivery system

The overall goal of this project was to design a novel drug delivery system to increase the stability in circulation, cellular permeability and cell-specific targeting of peptide drugs. This delivery system has therapeutic peptides containing hydrophobic tails which will self-assemble to form a micellular nanoparticle, and antibody fragments binding to the nanoparticle. My project focused on the antibody fragments of the delivery system, in which I used various molecular techniques to clone, express and isolate a scFv against CD19 expressed on normal and malignant B cells. I was also able to use flow cytometry to test the binding ability of purified scFv protein to CD19 on human lymphoma B cells and other controls. The flow cytometry indicated that the purified scFv fragment bound specifically to CD19 expressed on B cells.

- ***Research Assistant & Independent Study,*** Humphries Lab

Lawrence University, Appleton, WI Sept 2015-Jun.2016

During the academic year, I worked on two research projects. The first one was to investigate whether the TLR signaling pathway is involved in the regulation of immune-related genes in *B. glabrata,* which was not widely-studied yet. In this project, I used PCR and gel electrophoresis to examine transcriptional levels of different genes involved in the TLR pathway in the *B. glabrata* embryonic cell line (Bge cells). Results showed that genes involved in the TLR pathway are present in Bge cells, indicating the possible role of the TLR pathway in *B. glabrata* immunity. The second project was to use PCR and gel electrophoresis to determine whether Bge cells express Mpeg. During the project, I also helped to optimize the PCR protocol. Results showed that the Mpeg is transcribed in Bge cells, indicating its possible immunological role in *B. glabrata*. This project was also the starting point for my senior capstone project.

AWARDS & HONORS

Johns Hopkins Bloomberg School of Public Health Aug 2018

- MMI Departmental Tuition Fellowship

Lawrence University Aug 2013-Jun 2017

- 2016-2017 Dean's list
- Four-year International Student Scholarship
- 2017 Chandler Senior Experience Funds
- 2016 Summer Research Fellowship

MEMBERSHIP:

- American Society of Microbiology 2018-Present

PRESENTATIONS:

- **L. Wang,** J. Romano, I. Coppens. Investigating the Dynamics of the Interaction between Mammalian Host Organelles and *Toxoplasma*. Presented to The Delta Omega Scientific Poster Competition at Johns Hopkins Bloomberg School of Public Health; February 2019; Baltimore, MD.
- **L. Wang,** I. Coppens. Investigating the Dynamics of the Interaction between Mammalian Host Organelles and *Toxoplasma*. Presented to MMI Departmental Research Forum at Johns Hopkins Bloomberg School of Public Health; April 2018; Baltimore, MD.
- **L. Wang,** J. Humphries. Molecular characterization and immune responses of macrophage expressed gene from freshwater snail, *Biomphalaria glabrata*. Poster session presented at Senior Experience Symposium at Lawrence University; May 2017; Appleton, WI.
- **L. Wang,** M. R. Schnorenberg, J. LaBelle. Cloning of CD19 single chain variable fragment (scFv) for a new peptide-based therapeutic delivery system. Poster session presented at Summer Research Symposium at Lawrence University; Oct 2016; Appleton, WI.

OTHER WORK EXPERIENCES

- ***Immunology Content Tutor***, Center for Academic Success Jan 2017-Mar 2017
  Lawrence University, Appleton, WI
- ***Student Assistant***, Biological Stock Room Nov 2016-Jan 2017
  Lawrence University, Appleton, WI
- ***Chinese Content Tutor***, Center for Academic Success Sept 2014-June 2017
  Lawrence University, Appleton, WI

VOLUNTEER EXPERIENCES:

- ***Shelter volunteer***, Saving Paws Animal Rescue In., Sept 2013-Jun 2017
- ***English Tutor***, Fox Valley Literacy Council, Sept 2014-Jun 2016
- ***Volunteer***, St. Elizabeth Hospital, Sept 2014-Jun 2015

LEADERSHIPS:

- ***Publicity Chair***, People for Animal Welfare, Appleton, WI Sept 2015-Jun 2017
- ***Secretory***, Chinese Student Association, Appleton, WI Sept 2015-Jun 2016